DESIGN OF A WIND-TUNNEL ROLL-DAMPING BALANCE INCORPORATING EXTERNALLY PRESSURIZED GAS BEARINGS OPERATING AT LARGE FILM REYNOLDS NUMBERS

G. E. Burt

ARO, Inc.

October 1969

VON KÁRMÁN GAS DYNAMICS FACILITY
ARNOLD ENGINEERING DEVELOPMENT CENTER
AIR FORCE SYSTEMS COMMAND
ARNOLD AIR FORCE STATION, TENNESSEE

NOTICES

When U. S. Government drawings specifications, or other data are used for any purpose other than a definitely related Government procurement operation, the Government thereby incurs no responsibility nor any obligation whatsoever, and the fact that the Government may have formulated, furnished, or in any way supplied the said drawings, specifications, or other data, is not to be regarded by implication or otherwise, or in any manner licensing the holder or any other person or corporation, or conveying any rights or permission to manufacture, use, or sell any patented invention that may in any way be related thereto.

Qualified users may obtain copies of this report from the Defense Documentation Center.

References to named commercial products in this report are not to be considered in any sense as an endorsement of the product by the United States Air Force or the Government.

DESIGN OF A WIND-TUNNEL ROLL-DAMPING BALANCE INCORPORATING EXTERNALLY PRESSURIZED GAS BEARINGS OPERATING AT LARGE FILM REYNOLDS NUMBERS

G. E. Burt
ARO, Inc.

FOREWORD

The research presented herein was sponsored by the Arnold Engineering Development Center (AEDC), Air Force Systems Command (AFSC), Arnold Air Force Station, Tennessee, under Program Element 65401F, Program 876A, Project G226.

The work was done by ARO, Inc. (a subsidiary of Sverdrup & Parcel and Associates, Inc.), contract operator of AEDC, AFSC, under Contract F40600-69-C-0001. The work was conducted under ARO Project No. VT8002 from August 1966 to August 1969, and the manuscript was submitted for publication on August 15, 1969.

The report was submitted to the University of Tennessee Space Institute as partial fulfillment of the requirements for a Master of Science degree.

The author wishes to acknowledge the many ARO, Inc. personnel in the von Kármán Gas Dynamics Facility (VKF), AEDC, whose assistance was invaluable in the many facets of work necessary to obtain the information required for this study. First, the author is indebted to Dr. J. Lukasiewicz, former VKF Facility Chief and presently Associate Dean for Graduate Studies and Research at the Virginia Polytechnic Institute, Mr. C. J. Schueler and Mr. L. K. Ward for their permission to use the experimental work as material for the thesis. The author also appreciates the help of Mr. J. E. Atkins who did the detail design work, Mr. C. T. Bell for assistance with computer programming, and Mr. C. M. Howard and Mr. B. Cleveland who were responsible for the excellent fabrication of the redesigned gas bearing. Thanks are also due to Dr. F. Shahrokhi of The University of Tennessee Space Institute for his assistance in the preparation and review of the thesis.

This technical report has been reviewed and is approved.

Eugene C. Fletcher
Lt Colonel, USAF
AF Representative, VKF
Directorate of Test

Roy R. Croy, Jr.
Colonel, USAF
Director of Test

ABSTRACT

A roll damping, wind tunnel balance consisting of journal and thrust gas (N_2) lubricated bearings was designed for use in the von Kármán Gas Dynamics Facility's continuous flow tunnels at the Arnold Engineering Development Center. The balance was designed to be contained in a space envelope of 2.5 inches in diameter and 8.0 inches long. It was required to support a radial load of 350 pounds located ± 2 inches from the journal bearing center and a thrust load of 150 pounds. In order to meet these specifications, the bearings had to be designed with large gas film Reynolds numbers where the assumptions of laminar flow and negligible inertia of the gas used in lubrication theory may be invalid. An experimental investigation of the bearing resulting from the initial design showed it to have a turbulent gas film which caused an unexpected detrimental effect on load capacity. A more thorough theoretical analysis was conducted to determine the effects of turbulent flow on gas bearing load capacity. Another bearing was designed and fabricated to operate in the laminar flow regime which improved the operating characteristics and was in good agreement with laminar flow theory.

TABLE OF CONTENTS

CHAPTER PAGE

LIST OF FIGURES

FIGURE PAGE

NOMENCLATURE

a	Orifice radius (orifice compensated), in
a,b	Dimensions of rectangular thrust pad, in
A_{jk}	Matrix used in determining C_j^1, Equation (39a)
A_0	Orifice restricting area, Figure 3, page 9, in^2
c	Bearing clearance (gas film thickness) at $\varepsilon = 0$, in
C	Source strength
C^0, C^1	Zeroth ($\varepsilon = 0$) and first order source strengths respectively, Equation (17c)
C_D	Orifice discharge coefficient
d	Orifice diameter if inherent compensated or feeder hole diameter if orifice compensated, Figure 3, in
$\overline{d}$	Recess depth, Figure 3, in
D	Journal bearing diameter, in
$G(p_f/p_s)$	Mass flow function, Equation (7)
h	Bearing radial clearance (gas film thickness), in
H	Bearing dimensionless radial clearance, h/c
I	Model mass moment of inertia about its transverse axis, $in\text{-}lb\text{-}sec^2$
K	Bearing static stiffness, lb/in or in-lb/rad
L	Journal bearing length, in
L_1	Distance between journal bearing orifice rows, in

m	Mass flow rate through an orifice, lb-sec/in or model mass, lb-sec^2/in
m^0, m^1	Zeroth ($\varepsilon = 0$) and first order mass flow rates respectively, Equation (25), lb-sec/in
M	Total mass flow rate of a journal or thrust bearing, 2Nm, lb/sec or lb-sec/in
m_f''	Film mass flow rate per unit surface area at the feeding plane, lb-sec/in^3
m_z'	Film mass flow rate in the z direction per unit length normal to the flow, lb-sec/in^2
m_θ'	Film mass flow rate in the θ direction per unit length normal to the flow, lb-sec/in^2
N	Number of orifices in each plane for journal bearing and number of orifices per side of thrust bearing
p	Pressure, psia
p_a	Ambient pressure, psia
p_s	Supply pressure, psia
P	Dimensionless pressure, p/p_a
P_0, P_1	Dimensionless zeroth ($\varepsilon = 0$) and first order pressure, respectively, Equation (17a)
r	Thrust bearing radial coordinate or journal bearing radius, in
r_1	Outside radius of thrust bearing, in
r_2	Inside radius of thrust bearing, in

r_c Radius to thrust bearing orifice center $(\sqrt{r_1 r_2})$, in

R Thrust bearing dimensionless radial coordinate

Re Reynolds number, Equation (58)

Re^* Modified Reynolds number, Equation (57)

Re_t Reynolds number at which transition from laminar to turbulent flow begins

~~R~~ Gas constant, $in^2/sec^2\text{-}°R$

S_u Average value of the summation term in Equation (43) evaluated at (R, θ) values of $(1 + d/2r_c, 0)$, $(1 - d/2r_c, 0)$, $(1, d/2r_c)$, and $(1, -d/2r_c)$

S_0 Average value of the bracketed term in Equation (31) evaluated at $\xi = \xi_0 + d/D$ and $\xi = \xi_0 - d/D$

S_1 Sum of the average values of Equations (23a) and (23b) evaluated at (ξ, θ) values of $(\xi_0 + d/D, \theta_k)$ and $(\xi_0 - d/D, \theta_k)$

t Time, sec

T Gas film temperature, °R

T_{jk} Term used in calculating $(U_3)_k$, Equation (38)

T_ω Bearing angular viscous-damping-moment parameter, torque/ω, in-lb-sec/rad

u Gas film velocity in the θ direction or x direction, in/sec

U_1, U_2, U_3	Components of the product P_0P_1 (i.e., $P_0P_1 = U_1 + U_2 + U_3$), Equation (22)
V	Ratio of supply pressure to ambient pressure, p_s/p_a
V_m	Mean velocity, in/sec
w	Gas film velocity in the z direction, in/sec
W	Bearing load, lb
W´	Bearing load per unit circumferential length, lb/in
$\overline{W}$	Dimensionless load, equals $W/(p_s - p_a)$ LD for journal bearing and equals $W/\pi (r_1^2 - r_2^2)$ $(p_s - p_a)$ for thrust bearing
x,y,z	Cartesian coordinates, Figures 4 and 5, pages 17 and 28, in
$\bar{z}$	Location of journal bearing load with $\bar{z} = 0$ midway between the two bearings, in
X,Z	Dimensionless coordinates used in rectangular thrust bearing analysis, Equation (40a)
α	Exponent used in restrictor coefficient, Λ; equals 3 for orifice compensation and 2 for inherent compensation
γ	Specific heat ratio
Δ	Relative displacement of the bearing outer race with respect to the inner race, Figures 4 and 5, in

δ	Dirac delta function
ε	Bearing eccentricity, Δ/c
θ	Angular coordinate, Figures 4 and 5, pages 17 and 28, rad
Λ	Laminar flow restrictor coefficient, Equation (9a)
Λ_T	Turbulent flow restrictor coefficient, Equation (63a)
μ	Viscosity, lb-sec/in^2
ξ	Journal bearing dimensionless axial coordinate, z/r, Figure 4
ξ_0	Dimensionless axial coordinate of orifice centers, L_1/D
$\xi_>$	The larger of ξ and ξ_0
$\xi_<$	The smaller of ξ and ξ_0
ρ	Density, lb-sec/in^4
τ	Shear stress, lb/in^2
Ψ	Term used in mass flow derivative, Equation (27c)
ω	Angular velocity of the bearing outer race, rad/sec
ω_s	Steady state speed, rad/sec

Subscripts

a	Angular
A	Axial
f	Evaluated at the feeding plane
j	Evaluated at the j^{th} orifice
k	Evaluated at the k^{th} orifice
l	Laminar
r	Radial
t	At transition from laminar to turbulent flow
T	Turbulent

CHAPTER I

INTRODUCTION

Inferior performance and sometimes failures of re-entry vehicles (R/V) and sounding rockets because of the coupling of the roll and nutational frequencies and other roll associated phenomena has generated an increased interest in the dynamic characteristics of these vehicles. Thus a roll damping and Magnus force test mechanism (Figure 1) was designed and fabricated for use in the continuous flow wind tunnels of the Von Kármán Gas Dynamics Facility (VKF), Arnold Engineering Development Center (AEDC) so that experimental investigations could be performed to determine these roll characteristics. A complete description of these test mechanisms can be found in Reference [1][1].

A gas bearing was used as the balance in the roll damping test mechanism since it has very low frictional torque. The friction that does exist does not vary with age and is not a strong function of the load which makes a gas bearing very desirable for a wind tunnel balance. Other gas bearings have been used very successfully at the VKF as a

---

[1]Numbers in brackets refer to similarly numbered references in the bibliography.

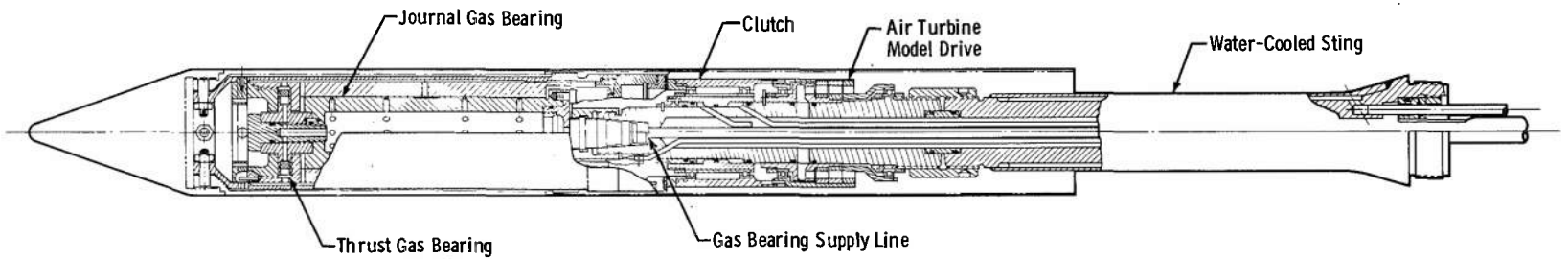

a. Roll damping test mechanism.

Note: All components of the two mechanisms are common except the balances which are interchangeable.

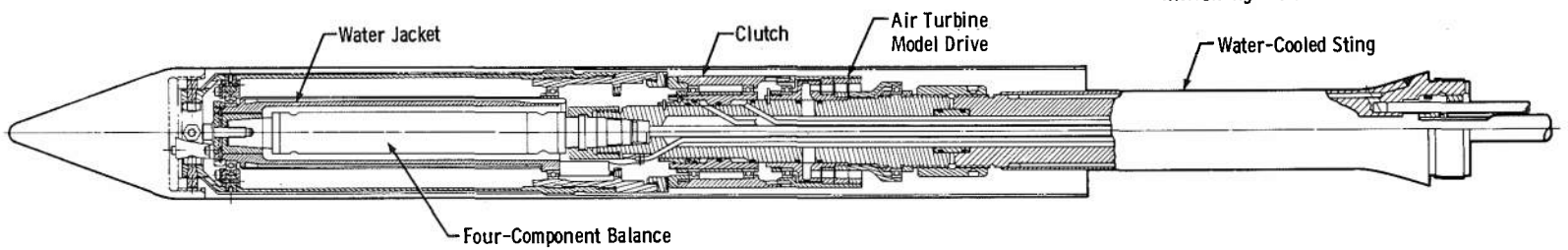

b. Magnus force test mechanism.

Figure 1. Dynamic Roll Balances used at the von Kármán Gas Dynamics Facility.

pitch damping balance (cylindrical bearing) and as a three-degree-of-freedom balance (spherical bearing) and are described in References [1], [2], and [3].

The gas bearing to be used for the roll damping balance was designed to be contained in a space of 2.5 inches in diameter and 8 inches in length. The balance was required to support both drag and lift loads, and since the center of pressure of the model could not be located exactly at the journal bearing center, the balance had to sustain pitching moment loads. After considering all the expected configurations to be tested along with possible tunnel conditions, it was determined that the balance should carry a radial load of 350 pounds located at ± 2 inches from the bearing center and an axial load of 150 pounds. The balance with a typical model attached must also remain dynamically stable at rotational speeds up to 5000 revolutions per minute.

This size and load specification required that the bearing operate in a regime where the viscous lubrication theory assumptions of laminar flow and negligible inertia terms in the Navier Stokes equations may be invalid. The purpose of this study is to cover the design of this roll damping, gas bearing balance with emphasis on the gas film turbulent flow regime which resulted in the initial design.

CHAPTER II

THEORETICAL ANALYSIS

The theory of gas film lubrication with external pressurization has been greatly refined since the first such gas bearing was built in 1904 by George Westinghouse. A history of gas film lubrication can be found in Reference [4]. Much of the theoretical advancement for these bearings has been made in the past decade. A brief summary of some of these more recent analyses will be given, and the theory used in this analysis will be presented.

Although there have been many different approaches to the analysis of gas bearings, the basic assumptions are the same and are listed below:

1. The inertia forces of the gas film are negligible.
2. The gas film is so thin that pressure, density, and viscosity may be considered constant across the film; and velocity gradients across the film are much larger than gradients along the film.
3. The gas film flow is laminar.
4. The gas film is isothermal.

I. ONE-DIMENSIONAL ANALYSIS

The cylindrical journal bearing shown in Figure 2, will be used to illustrate the different flow models that can be used in a theoretical analysis. Figure 2a shows a one-dimensional-flow (1D) model that has been used extensively in early gas film analysis.

Gas Film Analysis

The analysis of the flow in this model, which is an exact model for a journal bearing under no load and an infinite number of feeding orifices (line source feeding), is quite straight forward and is useful in illustrating the basic viscous lubrication theory. Based on the previously mentioned assumptions, the Navier Stokes equations for this case reduce to

$$\frac{\partial^2 w}{\partial y^2} = \frac{1}{\mu}\frac{\partial p}{\partial z} , \tag{1}$$

which can be integrated to give

$$w = \frac{1}{2\mu}\frac{\partial p}{\partial z} y(y-h) .$$

The mass flow per unit bearing width can be determined to be

$$m_z' = \int_0^h \rho\, w dy = -\frac{h^3}{12\mu}\rho\frac{\partial p}{\partial z} . \tag{2}$$

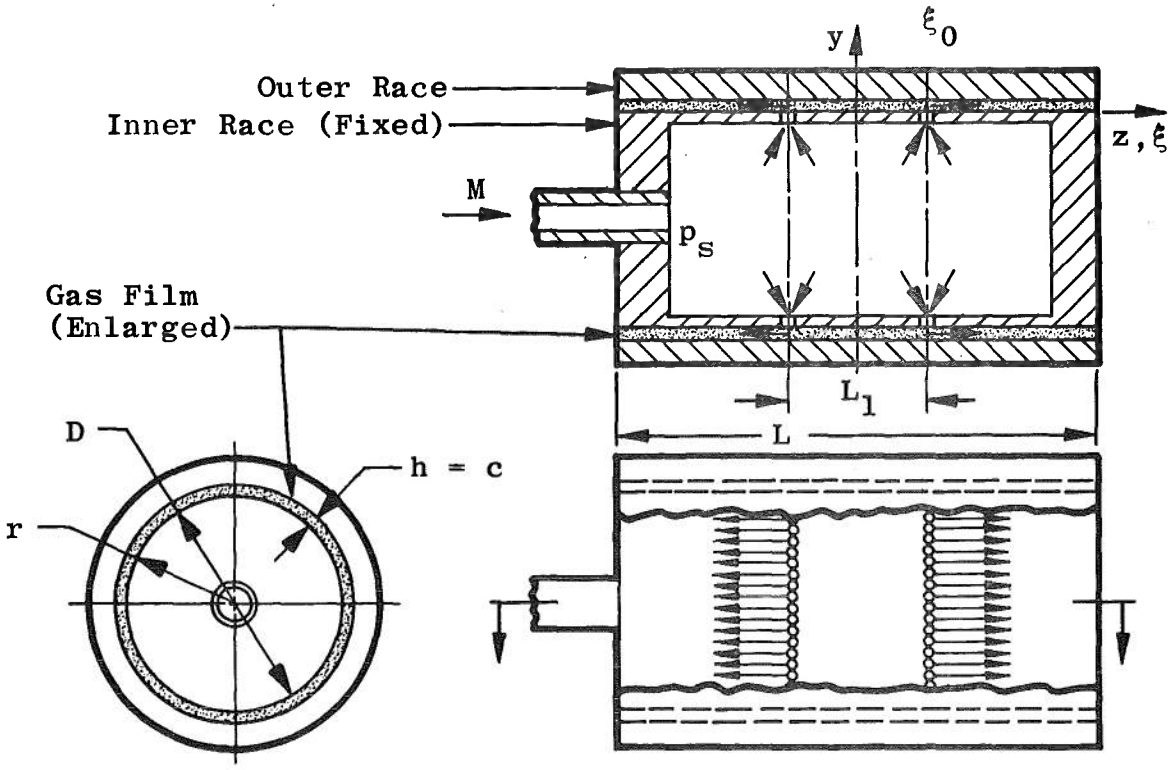

a. Unloaded bearing with line source feeding.

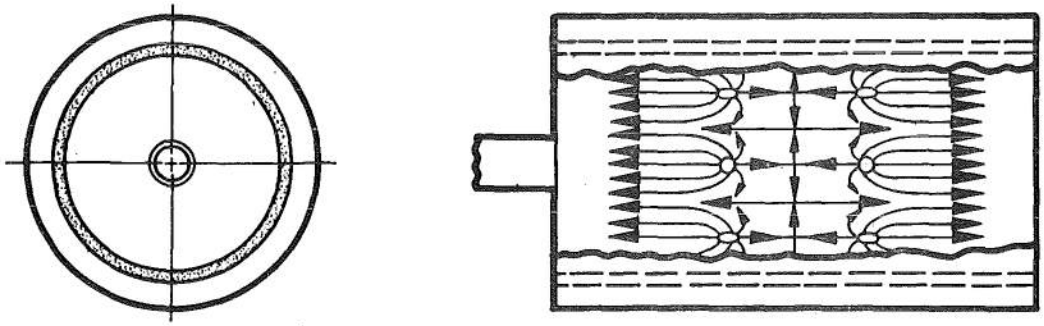

b. Unloaded bearing with point source feeding.

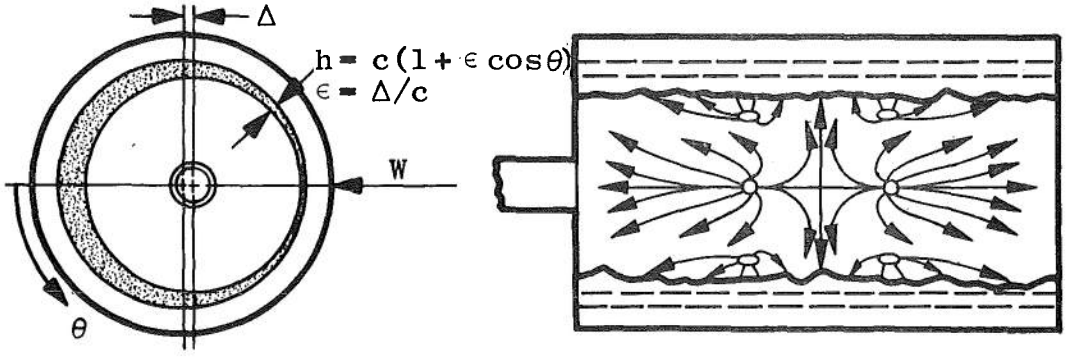

c. Loaded bearing with point source feeding.

Figure 2. Journal Bearing Flow Models.

Introducing the steady flow continuity equation results in the Reynolds equation for one-dimensional flow,

$$\frac{\partial}{\partial z}\left(-\frac{h^3}{12\mu}\rho\frac{\partial p}{\partial z}\right) = 0 \tag{3}$$

which describes the gas film outside the feeding plane.

Using the isothermal assumption in Equations (2) and (3) and integrating yields, respectively, in dimensionless form

$$P^2-1 = \frac{24\mu RT\, m'_z}{p_a^2\, h^3}\, r\left(\frac{L}{D} - \xi_>\right) \tag{4}$$

and

$$P = \left[\frac{P_f^2\left(\frac{L}{D} - \xi_>\right) + \left(\xi_> - \xi_0\right)}{\left(\frac{L}{D} - \xi_0\right)}\right]^{1/2} \tag{5}$$

where $\xi_>$ is the maximum of (ξ, ξ_0).

The load normal to the bearing surface per unit length in the θ direction can be determined by integrating the pressure, Equation (5), over the length, L, which gives

$$W' = \left\{P_f\left[1 - \frac{\left(1 - \frac{L_1}{L}\right)\left(3 + P_f\right)}{3\left(1 + P_f\right)}\right] - \left[\frac{1 + 2\left(\frac{L_1}{L}\right)}{3}\right]\right\} p_a L \,. \tag{6}$$

The only unknown in the above equations is P_f, the dimensionless pressure at the exit of the feeding plane, which

can be determined by matching the mass flow rate in the gas film with the flow introduced through the feeding holes.

Flow Restrictors

There are several types of inlet restrictors, most of which are described in Reference [5], that can be used to regulate the mass flow through the feeding plane; but only orifice type restrictors with adiabatic flow will be considered in this analysis. There are two types of restrictors, shown in Figure 3, that fall in this category. Figure 3a shows an "orifice compensated" configuration in which the restricting area is formed by the orifice cross-sectional area, whereas Figure 3b shows an "inherent compensated" configuration in which the restricting area is the curtain area formed by the edge of the orifice and the film thickness. The term, inherent compensation, was first introduced by Grinnel and Richardson [6]. The orifice compensated restrictor has better load characteristics than the inherent compensated restrictor, but it is subject to an instability known as "pneumatic hammer" as found in References [7], [8], and [9]. The inherent compensated restrictor does not experience this instability if there is no recess around the restrictor.

The orifice mass flow equation can be written as

$$m = \frac{C_D A_0 p_s}{\sqrt{RT}} G\left(\frac{p_f}{p_s}\right) , \qquad (7)$$

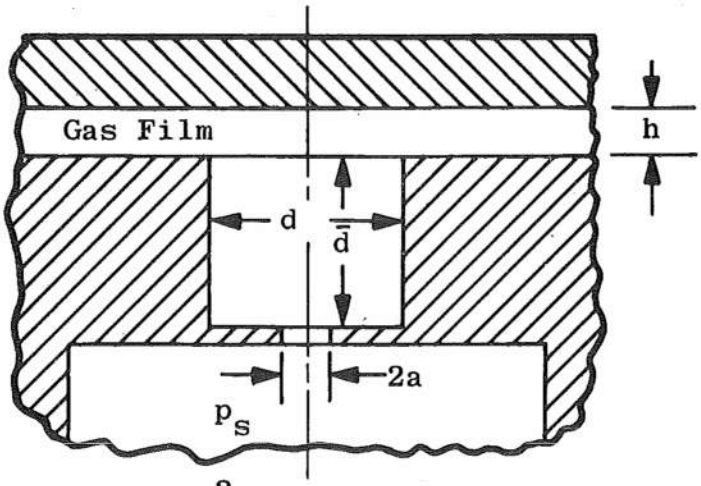

$$A_0 = \pi\ a^2 \ll \pi\ dh$$
$$\pi\ a^2 \ll 2\pi a\ (\bar{d} + h)$$

a. Orifice compensation.

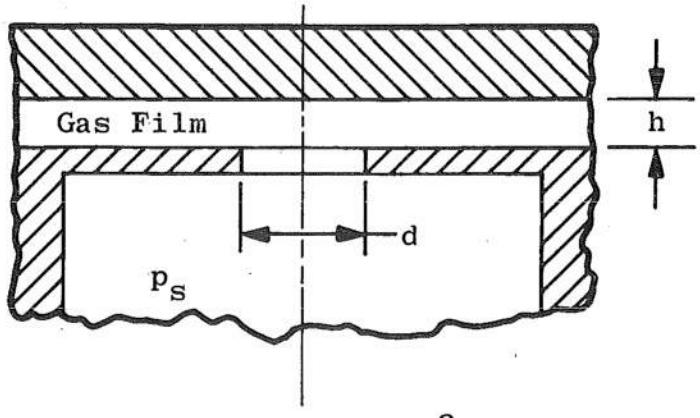

$$A_0 = \pi\ dh \ll \pi/4\ d^2$$

b. Inherent compensation.

Figure 3. Types of Orifice Restrictors.

where

$$G\left(\frac{p_f}{p_s}\right) = \left\{\frac{2\gamma}{\gamma-1}\left[\left(\frac{p_f}{p_s}\right)^{\frac{2}{\gamma}} - \left(\frac{p_f}{p_s}\right)^{\frac{\gamma+1}{\gamma}}\right]\right\}^{1/2}$$

when

$$\left(\frac{p_f}{p_s}\right) > \left(\frac{2}{\gamma+1}\right)^{\frac{\gamma}{\gamma-1}}$$

and

$$G\left(\frac{p_f}{p_s}\right) = \left[\gamma\left(\frac{2}{\gamma+1}\right)^{\frac{\gamma+1}{\gamma-1}}\right]^{1/2}$$

when

$$\left(\frac{p_f}{p_s}\right) \leq \left(\frac{2}{\gamma+1}\right)^{\frac{\gamma}{\gamma-1}} .$$

The area term, A_0, in Equation (7) can be written as

$$A_0 = \begin{cases} \pi a^2 \text{ ; orifice compensation} \\ \pi \text{ dh; inherent compensation.} \end{cases} \tag{8}$$

Equating Mass Flows

Evaluating Equation (4) at the feeding plane and equating the film mass flow rate to the orifice mass flow rate, Equation (7), yields

$$P_f^2 = \frac{2\Lambda V(L - L_1)\ (1 + \varepsilon \cos\ \theta)^{-\alpha}}{D}\ G\left(\frac{P_f}{V}\right) + 1\ , \qquad (9)$$

where

$$\Lambda = \frac{6C_D\ \mu N\sqrt{RT}}{p_a\ c^{\alpha}}\ (a^2)^{(\alpha-2)}\ (d)^{(3-\alpha)}\ , \qquad (9a)$$

$$\left.\begin{aligned} h &= c(1 + \varepsilon \cos\ \theta)\ , \\ \varepsilon &= \Delta/c\ , \end{aligned}\right\} \text{(Figure 2c, page 6)}$$

$$\alpha = \begin{cases} 3 \text{ for orifice compensation} \\ 2 \text{ for inherent compensation.} \end{cases}$$

The stiffness at $\varepsilon = 0$ can be determined by the relation,

$$\left.\frac{dW}{d\varepsilon}\right|_{\varepsilon=0} = R \int_0^{2\pi} \left.\frac{dW'}{dP_f}\ \frac{dP_f}{d\varepsilon}\right|_{\varepsilon=0} \cos\ \theta\ d\theta\ . \qquad (10)$$

The first derivative can be evaluated from Equation (5) in terms of P_f to give

$$\frac{1}{p_a\ L}\ \frac{dW'}{dP_f} \equiv D_1 = 1 - \frac{1 - \frac{L_1}{L}}{3}\left[1 + \frac{2}{(1 + P_f)^2}\right]\ . \qquad (11)$$

The second derivative in Equation (10) can be determined from Equation (9) to be

$$\frac{1}{\alpha \cos\theta}\left.\frac{dP_f}{d\varepsilon}\right|_{\varepsilon=0} \equiv D_2 = \frac{P_f^2 - 1}{2 P_f}\left\{1 - \frac{P_f^2 - 1}{2\gamma P_f^2}\left[1 + \frac{\gamma - 1}{2 - 2\left(\frac{V}{P_f}\right)\frac{(\gamma-1)}{\gamma}}\right]\right\}^{-1}, \tag{12}$$

where the term in braces is 1 for choked flow. Since D_1 and D_2 are independent of θ Equation (10) can be integrated to yield in dimensionless form

$$\left.\frac{d\bar{W}}{d\varepsilon}\right|_{\varepsilon=0} = \frac{\pi \alpha}{2(V - 1)} (D_1)\ (D_2) \tag{13}$$

which is a function of P_f. P_f can be related to Λ by using Equation (9) ($\varepsilon = 0$) and the stiffness can thus be determined as a function of the restrictor coefficient. Tang and Gross used a similar analysis and their design charts are presented in Reference [10]. It can be seen from Equation (13) that the stiffness of a gas bearing with inherent compensation is two-thirds the stiffness of the same configuration with orifice compensation for a fixed value of P_f.

Although the one-dimensional-flow analysis does provide a reasonably quick method to obtain rough design estimates for some bearing configurations, it usually predicts the optimum mass flow rate to be too large (too large orifice diameter) and overestimates load capacity by as much as 100 percent.

II. POINT SOURCE EFFECT

Gas bearing films are most often fed through discrete orifices (point source feeding) as shown in Figure 2b, page 6, rather than the line source discussed previously. This is the prime reason for the 1D analysis to predict orifice diameters too large for maximum stiffness. The point source effect has been investigated by Dudgeon and Lowe [11] using an analog analysis. The results from this investigation were used to provide corrections to the line source analysis. The analysis used in Reference [6] also used a line to point source correction, which was obtained from data presented in Reference [12]. These corrections help the one-dimensional-flow analysis to give more accurate predictions but it still usually overestimates the load capacity.

III. CIRCUMFERENTIAL FLOW EFFECT

When a load is applied to the journal bearing, the gas in the film begins to flow from the high pressure (small clearance) side of the bearing to the low pressure (large clearance) side as shown in Figure 2c, page 6. This flow tends to reduce the circumferential pressure gradient and thus load capacity predicted by the 1D analysis. The error introduced by ignoring the circumferential flow becomes larger as the bearing length to diameter ratio is increased.

Robinson and Sterry [13] and Shires [14] applied empirical corrections to account for the circumferential flow, Dudgeon and Lowe [11] used the average pressure obtained from the one-dimensional-flow analysis, applied this pressure to obtain the circumferential flow, and iterated to obtain the load capacity. Lund et al. [15] used an ε-perturbation, two-dimensional-flow (2D) analysis which will be discussed later to account for the circumferential flow. In one case this analysis was used with an empirical correction for the point source effect to give very good results. Extensive design data using this analysis are available in Reference [16]. In another case a more exact analysis, which will be used in this investigation, was obtained using the ε-perturbation technique considering point source flow.

IV. ε-PERTURBATION, POINT SOURCE JOURNAL BEARING ANALYSIS

Before the ε-perturbation analysis is applied, it is necessary to obtain the two-dimensional-flow Reynolds equation. Using the basic gas film assumptions, the Navier Stokes equation in the circumferential direction reduces to

$$\frac{\partial^2 u}{\partial y^2} = \frac{1}{\mu r} \frac{\partial p}{\partial \theta} ;$$

and similar to the 1D analysis, the circumferential velocity and mass flow rate per unit bearing length can be expressed as

$$u = \frac{1}{2\mu} \frac{\partial p}{r \partial \theta} y(y - h) ,$$

$$m'_\theta = - \frac{h^3}{12\mu} \rho \frac{\partial p}{r \partial \theta} . \qquad (14)$$

Using Equations (2) and (14) along with the continuity equation results in the Reynolds equation for two-dimensional-flow,

$$\frac{\partial}{\partial z} \left[\frac{h^3}{12\mu} \rho \frac{\partial p}{\partial z} \right] + \frac{1}{r^2} \frac{\partial}{\partial \theta} \left[\frac{h^3}{12\mu} \rho \frac{\partial p}{\partial \theta} \right] + \dot{m}''_f = 0 ,$$

where $\dot{m}''_f$ is the external mass flow rate per unit surface area. Using the isothermal assumption and introducing the dimensionless parameters,

$$P = \frac{p}{p_a} , \qquad H = \frac{h}{c} , \quad \text{and} \quad \xi = \frac{z}{r} ,$$

gives

$$\frac{\partial}{\partial \xi} \left[H^3 \frac{\partial P^2}{\partial \xi} \right] + \frac{\partial}{\partial \theta} \left[H^3 \frac{\partial P^2}{\partial \theta} \right] + \frac{24 r^2 \mu \, \mathcal{R}T}{c^3 \, p_a^2} \dot{m}''_f = 0 .$$

Since in this analysis the orifices are represented by point sources, the feeding term can be replaced by the source strength and the preceding equation becomes

$$\frac{\partial}{\partial \xi}\left[H^3 \frac{\partial P^2}{\partial \xi}\right] + \frac{\partial}{\partial \theta}\left[H^3 \frac{\partial P^2}{\partial \theta}\right] = - \delta(\xi - \xi_0) \sum_{j=1}^{N} C_j \, \delta(\theta - \theta_j) \, , \tag{15}$$

where

$\delta(\ )$ is the Dirac delta function,

ξ_0 is the ξ-coordinate of the point sources,

θ_j is the angular position of the j^{th} source,

N is the number of sources on each side of the origin

C_j is the strength of the j^{th} point source.

Since the bearing is symmetric in ξ, it is sufficient to consider only half of the bearing. An unfolded view of the bearing along with the coordinate system and boundary conditions is shown in Figure 4.

It is clear from Figure 4a that H can be expressed as

$$H = 1 + \varepsilon \cos \theta \tag{16}$$

where ε is defined as Δ/c. Now expanding P and C_j in power series of ε and omitting all terms in ε of second degree or higher gives

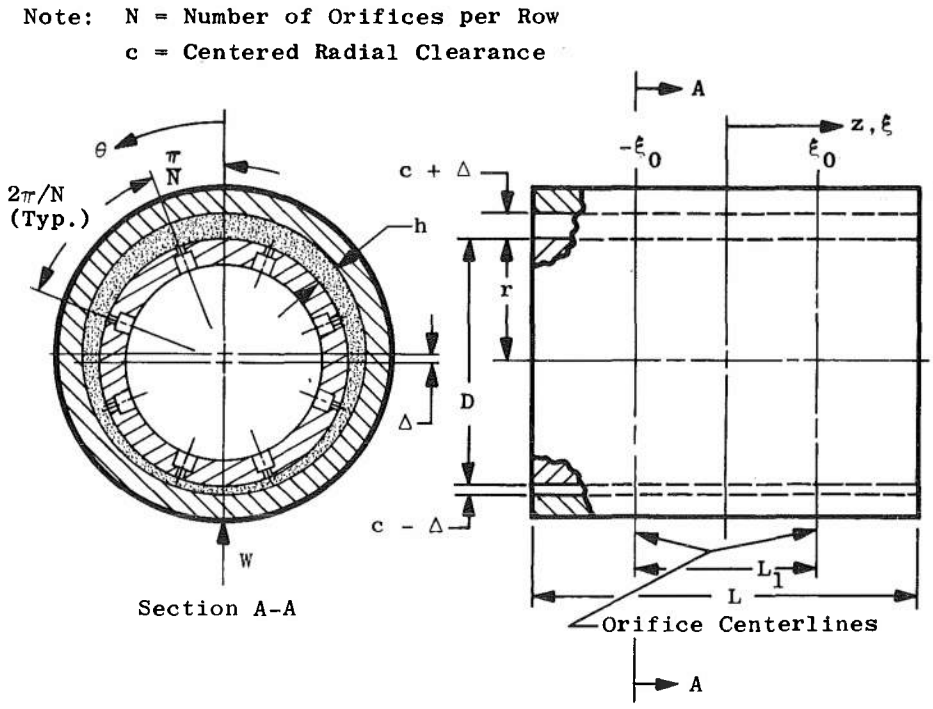

a. Bearing geometry.

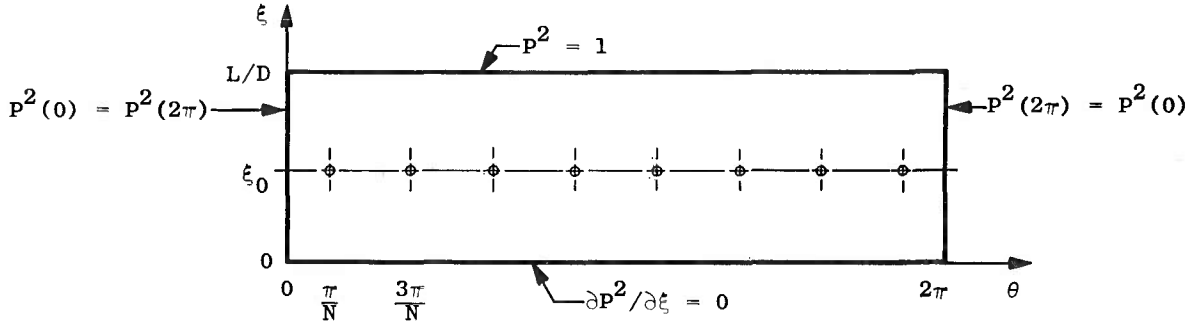

b. Unrolled view.

Figure 4. Journal Bearing Nomenclature and Boundary Conditions.

$$P^2 = P_0^2 + 2\varepsilon P_0 P_1 , \tag{17a}$$

$$H^3 = 1 + 3\varepsilon \cos\theta , \tag{17b}$$

$$C_j = C_j^0 + \varepsilon C_j^1 . \tag{17c}$$

Zeroth Degree Equation

Substitution of Equation (17) into Equation (15), omitting again the higher order terms of ε yields

$$\nabla^2(P_0^2) = - \delta(\xi - \xi_0) \sum_{j=1}^{N} C_j^0 \, \delta(\theta - \theta_j) \tag{18}$$

as the equation of the zeroth degree in ε where

$$\nabla^2(\ ) = \frac{\partial^2(\ )}{\partial\xi^2} + \frac{\partial^2(\ )}{\partial\theta^2} \quad . \tag{19}$$

Since this corresponds to the symmetric case ($\varepsilon = 0$, constant clearance), and the orifices are equally spaced, the values of C_j are identical ($= C^0$) for a uniform source pressure; and thus it is only necessary to consider the sector:

$$\frac{2(j - 1)\pi}{N} \leq \theta \leq \frac{2j\pi}{N} .$$

Therefore Equation (18) reduces to

$$\nabla^2(P_0^2) = - C^0 \, \delta(\xi - \xi_0) \, \delta(\theta - \theta_j) \tag{20}$$

with the boundary conditions

$$P_0^2 = 1 \qquad \text{at} \qquad \xi = \frac{L}{D} ,$$

$$\frac{\partial (P_0^2)}{\partial \xi} = 0 \qquad \text{at} \qquad \xi = 0 ,$$

$$P_0^2 \Big|_{\theta_i} = P_0^2 \Big|_{\theta_{i-1}}$$

where

$$\theta_i = \frac{2i\pi}{N} ; \qquad i = 1,2,3 \ldots, N .$$

The solution to the above equation was found in Reference [15] to be

$$P_0^2 = 1 + \frac{C^0}{\pi} \left\{ \frac{N}{2} \left(\frac{L}{D} - \xi_> \right) + \sum_{n=1}^{\infty} (-1)^n \frac{\cos(nN\theta) \cosh(nN\xi_<) \sinh\left[nN\left(\frac{L}{D} - \xi_>\right)\right]}{n \cosh\left(nN \frac{L}{D}\right)} \right\} , \tag{21}$$

where

$$\xi_< = \text{minimum of } (\xi, \xi_0)$$

$$\xi_> = \text{maximum of } (\xi, \xi_0)$$

First Degree Equation

The first degree terms in ε resulting from combining Equations (15) and (17) yield

$$\nabla^2(P_0P_1) = \nabla^2(U_1 + U_2 + U_3) \tag{22}$$

where

$$\nabla^2 U_1 = \frac{3}{2} \sin\theta \frac{\partial}{\partial\theta}(P_0^2) , \tag{22a}$$

$$\nabla^2 U_2 = \frac{3}{2} C^0 \cos\theta \, \delta(\xi - \xi_0) \sum_{j=1}^{N} \delta(\theta - \theta_j) , \tag{22b}$$

$$\nabla^2 U_3 = -\frac{1}{2} \delta(\xi - \xi_0) \sum_{j=1}^{N} C_j^1 \, \delta(\theta - \theta_j) , \tag{22c}$$

with the boundary conditions.

$$P_0P_1 = 0 \qquad \text{at} \quad \xi = \frac{L}{D} ,$$

$$P_0P_1\Big|_{\theta=0} = P_0P_1\Big|_{\theta=2\pi} ,$$

$$\frac{\partial}{\partial\xi}(P_0P_1) = 0 \quad \text{at} \quad \xi = 0 .$$

The solutions of the above equations were found in Reference [15] to be

$$U_1 = \frac{3NC^0}{4\pi} \sum_{m=1}^{\infty} (-1)^m \left\{ \frac{\cos\alpha_m\theta}{\alpha_m(2mN-1)} \left[\frac{mN \cosh(\alpha_m \xi_<) \sinh\alpha_m(\frac{L}{D} - \xi_>)}{\cosh(\alpha_m \frac{L}{D})} - \right.\right.$$

$$\left.\left. \frac{\alpha_m \cosh(mN\,\xi_<) \sinh mN(\frac{L}{D} - \xi_>)}{\cosh(mN \frac{L}{D})} \right] +$$

$$\frac{\cos \beta_m \theta}{\beta_m (2mN + 1)} \left[\frac{mN \cosh (\beta_m \xi_<) \sinh \beta_m (\frac{L}{D} - \xi_>)}{\cosh (\beta_m \frac{L}{D})} - \right.$$

$$\left. \frac{\beta_m \cosh (mN \xi_<) \sinh mN (\frac{L}{D} - \xi_>)}{\cosh (mN \frac{L}{D})} \right] \Bigg\} , \qquad (23a)$$

$$U_2 = - \frac{3NC^0}{4\pi} \left\{ \sum_{m=1}^{\infty} (-1)^m \left[\frac{\cos (\alpha_m \theta) \cosh (\alpha_m \xi_<) \sinh \alpha_m (\frac{L}{D} - \xi_>)}{\alpha_m \cosh (\alpha_m \frac{L}{D})} \right] + \right.$$

$$\left. \sum_{m=0}^{\infty} (-1)^m \left[\frac{\cos (\beta_m \theta) \cosh (\beta_m \xi_<) \sinh \beta_m (\frac{L}{D} - \xi_>)}{\beta_m \cosh (\beta_m \frac{L}{D})} \right] \right\} , \qquad (23b)$$

$$U_3 = \frac{1}{2\pi} \sum_{j=1}^{N} C_j^1 \left[\frac{1}{2} (\frac{L}{D} - \xi_>) + \right.$$

$$\left. \sum_{m=1}^{\infty} \frac{\cos (m \theta_j) \cos (m \theta) \cosh (m \xi_<) \sinh m (\frac{L}{D} - \xi_>)}{m \cosh (m \frac{L}{D})} \right] , \qquad (23c)$$

where

$$\alpha_m = mN - 1 ,$$

$$\beta_m = mN + 1 .$$

If the source strength, C^0, is known, P_0 can be calculated from Equation (21). Now if the perturbed source strengths, C_j^1, are known, the perturbed pressure, P_1, can be determined by summing U_1, U_2, and U_3 in Equation (23) and dividing by P_0.

Calculation of Source Strength

The film mass flow rate at the k^{th} source can be determined from the isothermal assumption and Equations (2) and (14) to be:

$$m_k = - \frac{p_a^2 c^3}{24\mu RT} \oint H^3 \frac{\partial}{\partial n} (P^2) \, ds \tag{24}$$

where $\frac{\partial}{\partial n}$ is the outward normal derivative and the integration is performed along a path enclosing the k^{th} source. Substituting the perturbation series, Equation (17), into Equation (24) yields

$$m_k = m_k^0 + \varepsilon m_k^1 \, , \tag{25}$$

where

$$m_k^0 = - \frac{p_a^2 c^3}{24\mu RT} \oint_k \frac{\partial}{\partial n} (P_0^2) \, ds \, , \tag{25a}$$

$$m_k^1 = - \frac{p_a^2 c^3}{24\mu RT} \oint_k \left[2 \frac{\partial}{\partial n} (P_0 P_1) + 3 \cos\theta \frac{\partial}{\partial n} (P_0^2) \right] ds \, . \tag{25b}$$

Applying Green's theorem and Equation (20) to the integral in Equation (25a) gives

$$\oint_k \frac{\partial}{\partial n} (P_0^2)\, ds = \iint \nabla^2 (P_0^2)\, d\theta d\xi = - C^0 ,$$

and by Green's theorem and Equation (22), the integral in Equation (25b) reduces to

$$\oint_k \left[2 \frac{\partial}{\partial n} (P_0 P_1) + 3 \cos \theta \frac{\partial}{\partial n} (P_0^2) \right] ds = - C_k^1 .$$

Therefore Equation (25) can be written as

$$m_k = \frac{p_a^2 c^3}{24 \mu \cancel{RT}} (C^0 + \varepsilon C_k^1) . \tag{26}$$

Expanding the orifice mass flow in a Taylor's series about $P\big|_f = P_0\big|_f$ and $h = c$, omitting the f for clarity, gives

$$m_k(P,h) = m_k(P_0,c) + (P - P_0) \left.\frac{\partial m_k}{\partial P}\right|_{P_0,c} + (h - c)_k \left.\frac{\partial m_k}{\partial h}\right|_{P_0,c} \tag{27}$$

The derivatives in the above equation can be determined from Equation (7) and Equation (8) to be

$$\left.\frac{\partial m_k}{\partial P}\right|_{P_0,c} = m_k(P_0,c)\ \Psi/V , \tag{27a}$$

$$\left.\frac{\partial m_k}{\partial h}\right|_{P_0,c} = \begin{cases} 0, \text{ orifice compensation} \\ m_k(P_0,c)/c; \text{ inherent compensation} , \end{cases} \tag{27b}$$

where

$$\Psi = \frac{\left.\frac{d(C_D)}{dP}\right|_{P=P_0}}{C_D} + \frac{1}{\gamma}\left\{\frac{1}{\frac{P_0}{V}} - \frac{\gamma-1}{2\left(\frac{P_0}{V}\right)^{\frac{1}{\gamma}}\left[1 - \left(\frac{P_0}{V}\right)^{\frac{(\gamma-1)}{\gamma}}\right]}\right\} \tag{27c}$$

and the term in braces is zero for choked flow. Since $(P - P_0)_k$ is $\varepsilon P1_k$ and $(h - c)$ is $c\varepsilon(\cos\theta)$, Equation (27) can be written as

$$m_k(P,h) = m_k(P_0,c) + \varepsilon P1_k \, m_k(P_0,c)\,\Psi/V + (3-\alpha)\,\varepsilon\cos\theta\, m_k(P_0,c). \tag{28}$$

Equating the constant terms of Equations (26) and (28) and using Equation (7) to evaluate $m_k(P_0,c)$ gives

$$\Lambda V \, G\left(\frac{P_0|_f}{V}\right) = \frac{N}{4\pi} c^0 . \tag{29}$$

The angular location of the k^{th} source can be written as

$$\theta = \frac{\pi(2k - 1)}{N} . \tag{30}$$

Substituting this into Equation (21) yields

$$P_0^2\Big|_{\theta_k} = 1 + \frac{C^0}{\pi}\left[\frac{N}{2}\left(\frac{L}{D} - \xi_>\right) + \sum_{n=1}^{\infty} \frac{\cosh(nN\ \xi_<)\ \sinh\ nN\left(\frac{L}{D} - \xi_>\right)}{n\ \cosh\left(nN\ \frac{L}{D}\right)}\right] \tag{31}$$

Now to determine P_0 at the edge of the feeder hole, the term in brackets is first evaluated at $\xi = \xi_0 + (d/D)$; then it is evaluated at $\xi = \xi_0 - (d/D)$; and the two values are averaged. Defining this value as S_0, Equation (31) can be written as

$$P_0^2\Big|_f = 1 + \frac{C^0}{\pi}\ S_0 \tag{32}$$

C^0 can be determined by a simultaneous solution of Equations (29) and (32).

Now equating the coefficients of ε in Equations (26) and (28) and again evaluating $m_k(P_0,c)$ from Equation (7) yields

$$\Lambda V\ G\left(\frac{P_0}{V}\right)\left[P_{1_k}\frac{\Psi}{V} + (3-\alpha)\ \cos\ \theta_k\right] = \frac{N}{4\pi}\ C_k^1\ . \tag{33}$$

Introducing Equation (29) into the above equation gives

$$C^0\left[P_{1_k}\frac{\Psi}{V} + (3-\alpha)\ \cos\ \theta_k\right] = C_k^1 \tag{34}$$

where C^0 is a known value. Multiplying Equation (34) by P_0, substituting for θ_k from Equation (30), and rearranging yields

$$(P_0P_1)_k = \frac{P_0 V}{\Psi C^0} C_k^1 - (3-\alpha) \frac{P_0 V}{\Psi} \cos \frac{\pi(2k - 1)}{N} . \quad (35)$$

$(P_0P_1)_k$ can be obtained from Equation (23) to be

$$(P_0P_1)_k = (S_1)_k + (U_3)_k , \quad (36)$$

where $(S_1)_k$ is the sum of U_1 and U_2 which have been evaluated at $(\xi_0 + d/D, \theta_k)$ and $(\xi_0 - d/D, \theta_k)$, and the values averaged. Substituting $\pi(2j - 1)/N$ for the angular coordinate of the j^{th} source, θ_j, along with Equation (30) into Equation (23c) yields

$$(U_3)_k = \sum_{j=1}^{N} T_{jk} C_j^1 , \quad (37)$$

where

$$T_{jk} = \frac{1}{2\pi}\left[\frac{1}{2}\left(\frac{L}{D} - \xi_>\right) + \sum_{m=1}^{\infty} \frac{\cos \frac{m\pi(2j - 1)}{N} \cos \frac{m\pi(2k - 1)}{N} \cosh m \xi_< \sinh m\left(\frac{L}{D} - \xi_>\right)}{m \cosh \left(m \frac{L}{D}\right)}\right] \quad (38)$$

which can also be evaluated at $(\xi_0 + d/D)$ and $(\xi_0 - d/D)$ and averaged. Combining Equations (35) through (38) yields the following system of N linear equations:

$$A_{jk} C_j^1 = B_k , \quad (39)$$

where

$$A_{jk} = T_{jk} - \delta_{jk} \frac{P_0 V}{C^0 \Psi} ; \quad \delta_{jk} = \begin{cases} 0 \text{ if } j \neq k \\ 1 \text{ if } j = k \end{cases} \tag{39a}$$

$$B_k = - (S_1)_k - (3-\alpha) \frac{P_0 V}{\Psi} \cos \frac{\pi(2k - 1)}{N} . \tag{39b}$$

Thus the values of C_j^1 can be determined by the use of matrix albegra.

Now with the source strengths known the pressures can be obtained at any location. A numerical area integration can be performed on $(P_1 \cos \theta)$ to obtain the bearing stiffness, (load/ε). Although the ε-perturbation analysis is valid for small ε only, the stiffness of journal bearings is usually constant up to $\varepsilon = 0.5$.

V. THRUST BEARING ANALYSIS

The theoretical analysis of thrust bearings has also been improved during the past decade by using more exact mathematical models. More exact solutions of the gas film equations can be obtained for thrust bearings than journal bearings because the film thickness is not a function of the bearing coordinates. An analysis of a point source fed thrust bearing from Reference [15] will be used in this study. Figure 5 shows a double acting (two sided)

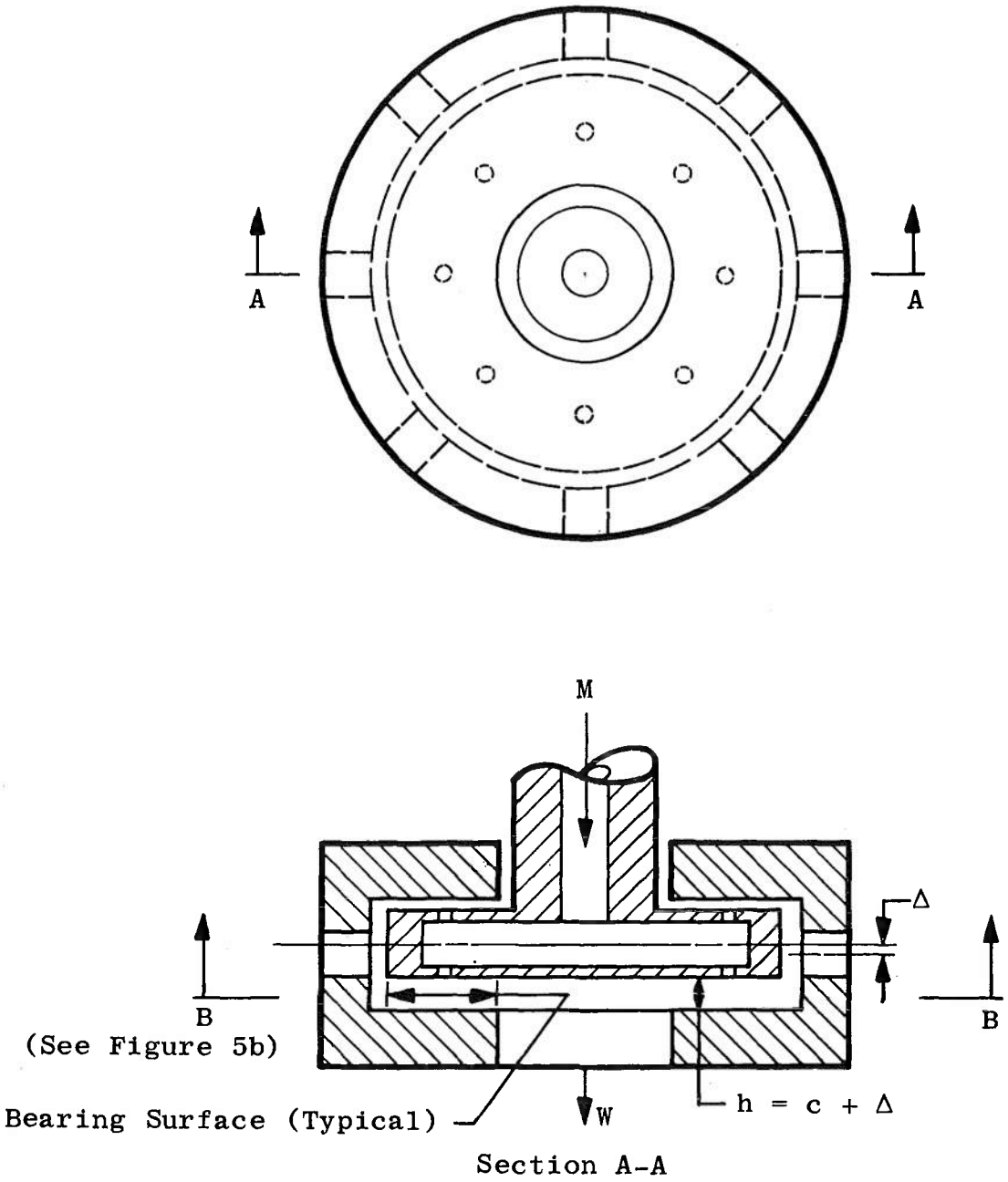

a. Bearing geometry.

Figure 5. Thrust Bearing Nomenclature and Boundary Conditions.

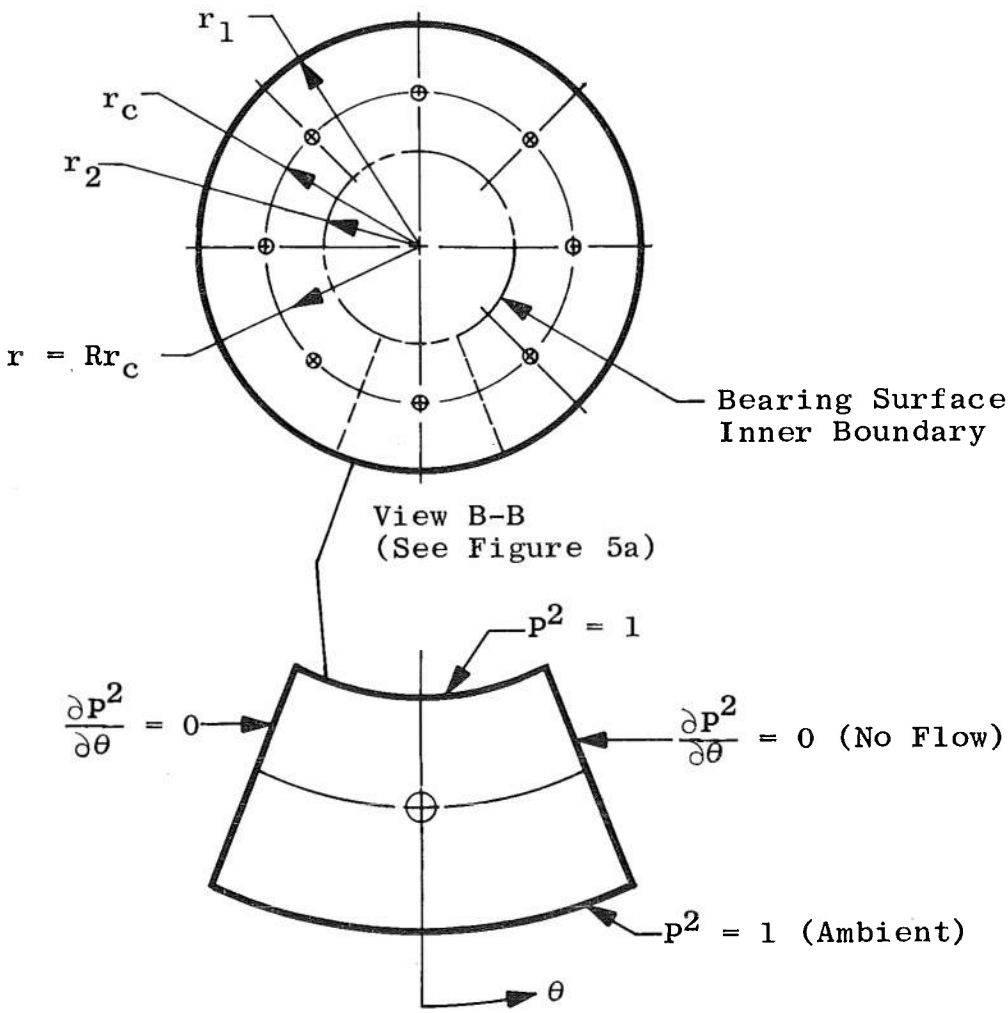

b. Radial pad.

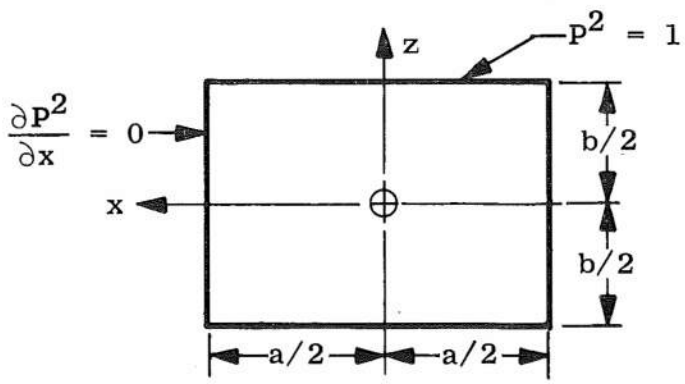

c. Rectangular pad.

Figure 5. (continued)

thrust bearing model with the nomenclature used in this analysis. It is assumed that the orifices are equally spaced; thus, it is only necessary to analyze one radial segment of the bearing as shown in Figure 5b.

Solution of Reynolds Equation

The solution to the gas film equation in the radial segment is found in Reference [15] by first solving the Reynolds equation for a rectangular pad as shown in Figure 5c and then using methods of conformal mapping to transform the rectangular pad into the radial segment. The Reynolds equation describing the gas film in the rectangular pad outside the feeding hole is

$$\frac{\partial^2 (P^2)}{\partial Z^2} + \frac{\partial^2 (P^2)}{\partial X^2} = 0 \ , \tag{40}$$

where

$$Z = z/a \ ,$$

$$X = x/a \ ,$$

with boundary conditions,

$$P^2 = 1 \qquad \text{at} \qquad Z = \pm \frac{b}{2a}$$

$$\frac{\partial (P^2)}{\partial X} = 0 \qquad \text{at} \qquad X = \pm \frac{1}{2}$$

as shown in Figure 5c. The external boundary conditions can be satisfied by superimposing the Laplacian solution of an

infinite number of equidistant (separated by a distance, a) sources distributed along the x axis and the Laplacian solution of an infinite number of equidistant (separated by a distance, b) alternate sources and sinks distributed along the z axis. The resulting pressure distribution is

$$P^2 = 1 - \frac{1}{2} C \sum_{n=-\infty}^{\infty} (-1)^n \ln \left[\frac{\cosh 2\pi \left[Z + n\left(\frac{b}{a}\right) \right] - \cos 2\pi X}{\cosh \left[\pi \left(\frac{b}{a}\right) (2n + 1) \right] - 1} \right], \quad (41)$$

where C is the source strength.

The rectangular pad can be transformed into the radial segment shown in Figure 5b using the transformation:

$$Z = \frac{N}{2\pi} \ln R , \quad (42a)$$

$$X = \frac{N}{2\pi} \theta , \quad (42b)$$

where N is the number of orifices and R is the dimensionless radius (r/r_c). The pressure in the radial segment can thus be written as

$$P^2 = 1 - \frac{1}{2} C \sum_{n=-\infty}^{\infty} (-1)^n \ln \left\{ \frac{\cosh N \left[\ln R + n \ln \left(\frac{r_1}{r_2}\right) \right] - \cos N\theta}{\cosh \left[N\left(n + \frac{1}{2}\right) \ln \left(\frac{r_1}{r_2}\right) \right] - 1} \right\} . \quad (43)$$

Since the orifice was located at the center of the rectangular pad, the transformation given in Equation (42a)

evaluated at (Z,R) equal to (b/2a, r_1/r_c) and (- b/2a, r_2/r_c) results in

$$r_c = \sqrt{r_1 r_2} \tag{44}$$

An analysis of a pad in which the orifice is not centered is given in Reference [15]; however, it will not be considered here.

Calculation of the Source Strength

Since the clearance, H, is constant, the mass flow per segment can be determined from Equation (24) to be

$$m_k = - \frac{p_a^2 h^3}{24\mu RT} \oint_k \frac{\partial}{\partial n} (P^2) \, ds \, . \tag{45}$$

If the integration is performed along the boundary of the rectangular pad, the above equation reduces to

$$m_k = - \frac{p_a^2 h^3}{12\mu RT} \int_{-\frac{1}{2}}^{\frac{1}{2}} \frac{\partial (P^2)}{\partial Z} \bigg|_{Z=\frac{b}{2a}} dX \, .$$

Evaluating the derivative in the preceding equation from Equation (41) yields

$$m_k = \frac{p_a^2 h^3 \pi}{12\mu RT} C \, . \tag{46}$$

The clearance, h, can be written as

$$h = c(1 \pm \varepsilon) \, , \tag{47}$$

where c is the clearance in the centered position, and ε is Δ/c as shown in Figure 5a, page 28. The term, $(1 + \varepsilon)$, is used for the larger gap side and $(1 - \varepsilon)$ is used for the smaller gap side. Combining Equations (46), (47) and (7) (evaluated at the orifice exit) gives

$$\frac{2\Lambda\ V\ G\left(\frac{P_f}{V}\right)}{N(1 \pm \varepsilon)^{\alpha}} = C \ , \tag{48}$$

where

$$\alpha = \begin{cases} 3; \text{ orifice compensation} \\ 2; \text{ inherent compensation.} \end{cases}$$

Now evaluating Equation (43) at the edge of the orifice gives

$$(P^2)_f = 1 - \frac{1}{2}\frac{C}{\pi}(S_u) \ , \tag{49}$$

where S_u is the value obtained from the summation term of Equation (43) evaluated at the orifice edge. The value of C can be obtained by a simultaneous solution of Equations (48) and (49). A value of C is determined for each side of the bearing and thus the pressure distribution on each side can be calculated from Equation (43). The pressure can be numerically integrated to obtain the load on each side and the difference gives the load capacity of the bearing at a given ε.

VI. COMPUTER PROGRAMS

The resulting solutions from the journal and thrust bearing analyses presented in the two preceding sections involve very complex equations with iterative processes necessary to determine the source strengths. Thus to be of any practical use, the equations must be solved by means of a digital computer. Computer program listings obtained from an IBM 704 computer are given in Reference [15] for these analyses. Some modifications were made to these programs and they were adapted for use on the CDC 1604-B computer located at the VKF. The modifications involved correcting several errors in the journal bearing analysis and adding the capability to make the computations for inherent compensated bearings (i.e., the last term in Equation (27) was added). The theoretical correction of two-thirds found in the 1D analysis to correct orifice compensation to inherent compensation produces the same load results as the present analysis but does not define the actual flow obtained.

The program given in Reference [15] for the thrust bearing did not have the capability to compute the source strength which was an input to the program. This was added in such a manner that both inherent and orifice compensated bearings could be analyzed.

VII. DYNAMIC ANALYSIS

Stability Criteria

Lund [7] shows that the additional bearing stiffness obtained from the "squeeze film" effect is negligible for externally pressurized bearings operating at moderate spin rates and large supply pressures, while Pan [17] shows for these conditions that the additional stiffness obtained from the "hydrodynamic" effect can also be neglected. Thus the first natural frequencies in the bearings considered herein can be calculated using

$$\omega_r = \sqrt{K_r/m} \quad , \tag{50a}$$

$$\omega_A = \sqrt{K_A/m} \quad , \tag{50b}$$

$$\omega_a = \sqrt{K_a/I} \quad . \tag{50c}$$

Film damping data are also presented in Reference [7] in graphical form such that one can estimate if a bearing can operate at (or pass slowly through) the natural frequency with a given amount of unbalance.

Friction Torque

The rolling friction (i.e., tare for roll damping balance) between the stationary and movable parts of the bearing can be determined from Newtons law of friction,

$$\tau_\theta = \mu \frac{\partial u}{\partial y} \quad . \tag{51}$$

The velocity distribution in the θ direction generated from the external pressurization is neglected since this effect would be integrated out during the following analysis due to symmetry. Thus Couette flow is obtained and the velocity distribution for the journal and thrust bearings is

$$u = r\,\omega\,(y/h) \quad , \tag{52}$$

where ω is the angular velocity of the rotating part of the bearing and y is the coordinate normal to the bearing surface.

Since $h = c\,(1 + \varepsilon \cos\theta)$ for the journal bearing, Equations (51) and (52) can be combined to give

$$\tau_\theta = \frac{r\,\omega\,\mu}{c(1 + \varepsilon \cos\theta)} \quad . \tag{53}$$

Integrating $(r\,\tau_\theta)$ over the bearing surface produces the angular viscous damping-moment parameter,

$$T_\omega = \frac{2\pi\, r^3\, \mu\, L}{c\sqrt{1 - \varepsilon^2}} \quad \text{(journal)} \quad . \tag{54}$$

Since $h = c(1 \pm \varepsilon)$ for the thrust bearing, combining Equations (51) and (52) yield

$$\tau_\theta = \frac{r\,\omega\,\mu}{c(1 + \varepsilon)} + \frac{r\,\omega\,\mu}{c(1 - \varepsilon)} \quad . \tag{55}$$

Integration of $(r\,\tau_\theta)$ over the bearing surface gives

$$T_\omega = \frac{\pi\,\mu(r_1^4 - r_2^4)}{c(1 - \varepsilon^2)} \quad \text{(thrust)} \quad . \tag{56}$$

CHAPTER III

DESIGN PROCEDURE

The gas bearing balance was to be contained in a space envelope of 2.5 inches in diameter and 8.0 inches in length. It was required to support a radial load of 350 pounds, located ± 2.0 inches from the journal bearing center, and an axial load of 150 pounds. It must also remain dynamically stable at rotational speeds up to 5000 revolutions per minute with a typical model installed.

In order to have a very rigid outer race for the journal bearing and to stay within the aforementioned space envelope, the journal bearing inner race diameter, D, was selected to be 1.80 inches. The total length of the journal bearing was limited to 6.00 inches since the remaining length was needed for the thrust bearing. With the space available, the maximum thrust bearing size was an outside diameter, $2r_1$, of 2.10 inches and an inside diameter, $2r_2$, 1.05 inches. Nitrogen was used as the lubricant.

I. JOURNAL BEARING DESIGN

In order to support the moment loading, it was decided to make two journal bearings of length, 2.70 inches, separated by 0.60 inch long undercut to vent the mass flow between the bearings (Figure 6). Since the journal bearing

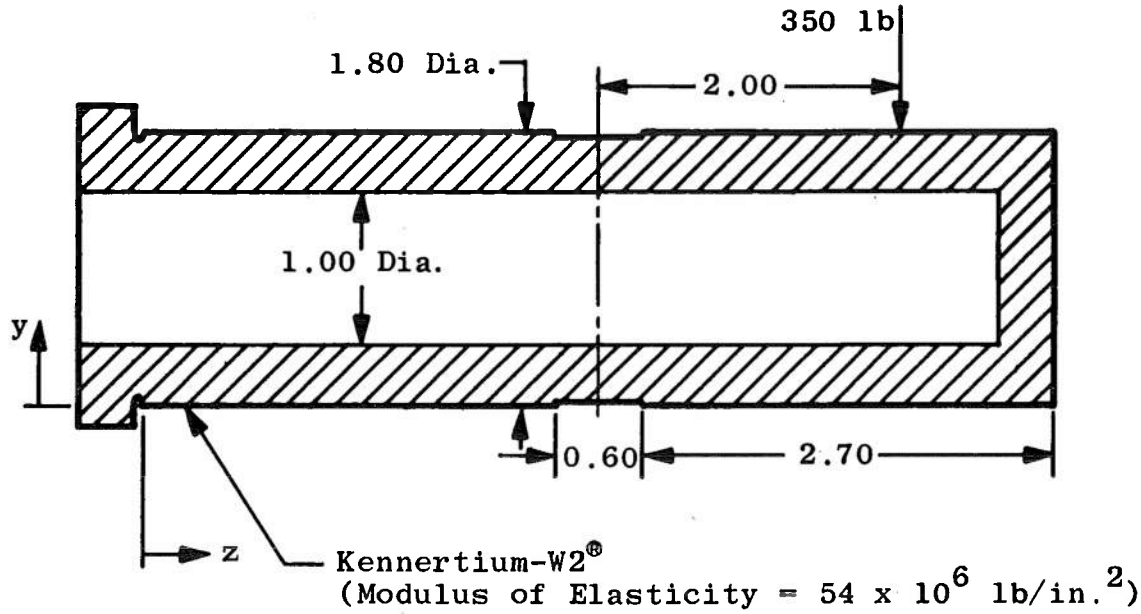

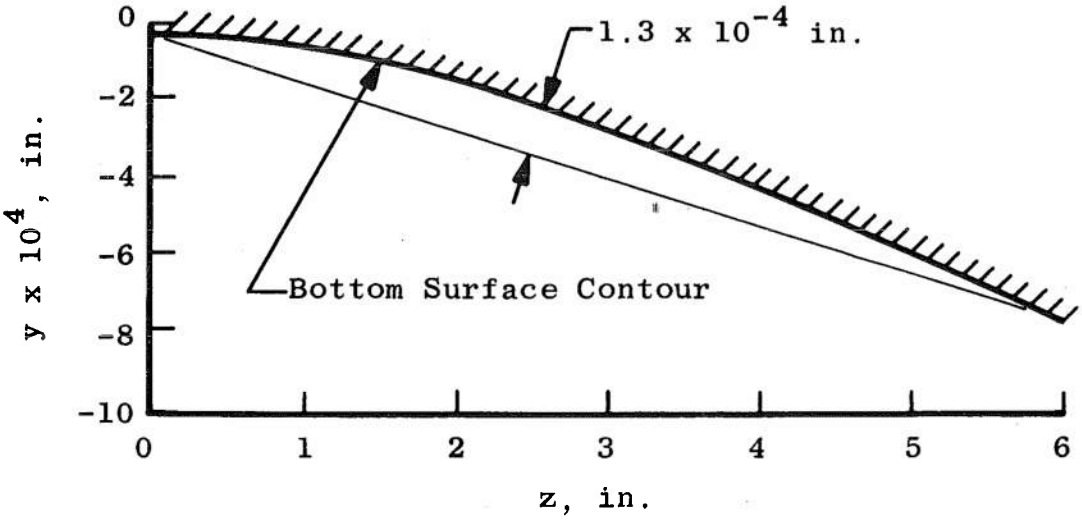

Figure 6. Surface Deflection of Journal Bearing Inner Race with Maximum Loading.

inner race has a reasonably small diameter for such large loads, the structural bending had to be considered. Kennertium-W2R[1] was the material selected for this part because it had a large modulus of elasticity, 54×10^6 lb/in^2 was dimensionally stable, and reasonably easy to machine. Figure 6 shows that even with the high stiffness material, the bending under maximum load is significant when considering the small clearances required for gas bearings. The outer shell has essentially no deflection, and therefore, 1.3×10^{-4} inches of the clearance is taken up by deflection.

Circumferential Orifice Spacing

Figure 7 shows the effect of the circumferential spacing of the orifices on the dimensionless stiffness, $\bar{W}/\varepsilon$, with the mass flow rate held constant. The load capacity increases as the number of orifices is increased up to about six. For larger numbers of orifices the load remains constant. Eight orifices per plane was selected for the present design.

Reynolds Number

As mentioned earlier, the theoretical analysis used assumed negligible inertia terms and laminar flow. For these assumptions to be true the Reynolds number must be held below a given value. In particular, the inertia

---

[1]R indicates registered trademark

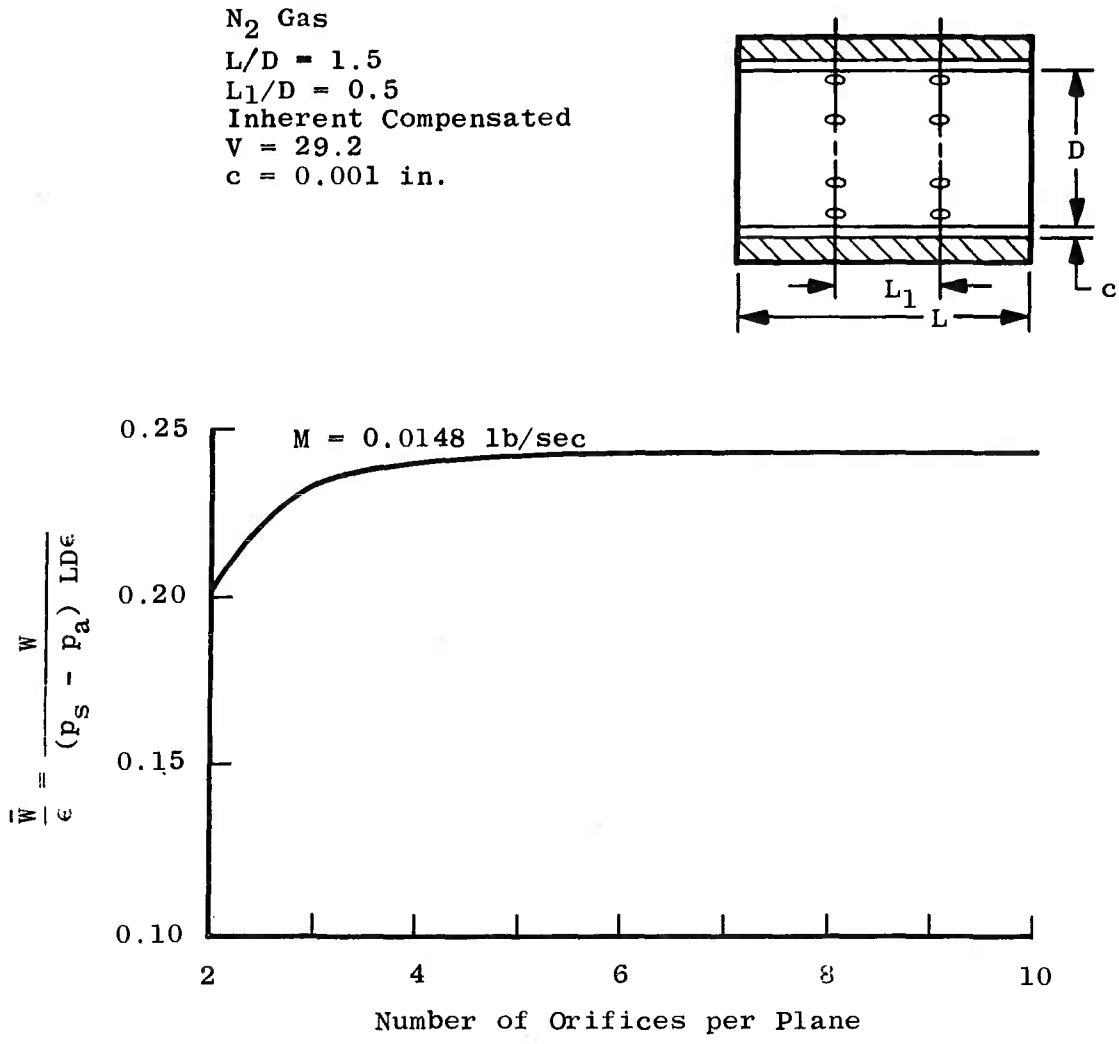

Figure 7. Effect of Circumferential Orifice Spacing on Load Capacity at Constant Mass Flow Rate for a Typical Configuration.

effects can be ignored if the modified Reynolds number, Re^*, is much less than one, where Re^* can be defined in terms of the Reynolds number, Re, to be

$$Re^* = Re\left(\frac{2h}{L - L_1}\right) , \tag{57}$$

with

$$Re = \rho V_m h/\mu , \tag{58}$$

V_m = the average velocity across the film.

Gross [18] states that the error due to neglecting inertia effects is only about 10 percent for $Re^* = 500$ and about 30 percent when $Re^* = 3500$.

The Reynolds number at which transition from laminar to turbulent flow begins is vague. Constantinescu [19] suggests that $Re_t = 500$; Gross [20] suggests $Re_t = 1000$; and Shires [21] in an experimental investigation with line source fed, one-dimensional flow, parallel plates found that $Re_t = 1300$ when h was .003 inch and Re_t increased slightly as h decreased. The bearing reported in Reference [2] has been operated with a double plane admission inner race at a Reynolds number of 1100 with a laminar film. It is desired to stay in the laminar flow regime not only to be able to apply the laminar theory but to keep the bearing friction torque small. When turbulent flow exists, the effective viscosity is increased and thus the friction torque is increased as shown in Equation (54).

The Reynolds number as given in Equation (58) can be expressed in terms of mass flow rate as

$$Re = M/2\pi\ D\mu\ , \tag{59}$$

since

$$M = 2\ \rho\ V_m\ \pi\ Dh\ .$$

Restrictor Coefficient Effect

The effect of the restrictor coefficient, Λ, on the dimensionless stiffness is given in Figure 8. The restrictor coefficient is essentially a measure of the ratio of the flow resistance of the gas film to the flow resistance of the inlet orifices. The curve shown is actually for the finally selected design. A family of similar curves can be obtained by changing the parameters listed on Figure 8. If a particular bearing has a "reasonable" number of orifices, the parameters in Column I (Figure 8) are fixed and the abscissa changed to Λ/V, the family of curves practically collapse into the curve shown, especially for values of V greater than five. If the stiffness is multiplied by 1.5, the curve also applies to orifice compensation. Numerous design charts are presented in Reference [16] in this form over an extended range of Λ/V.

The characteristic maximum in the curve is explained well in [14]. Briefly, if there is very little pressure

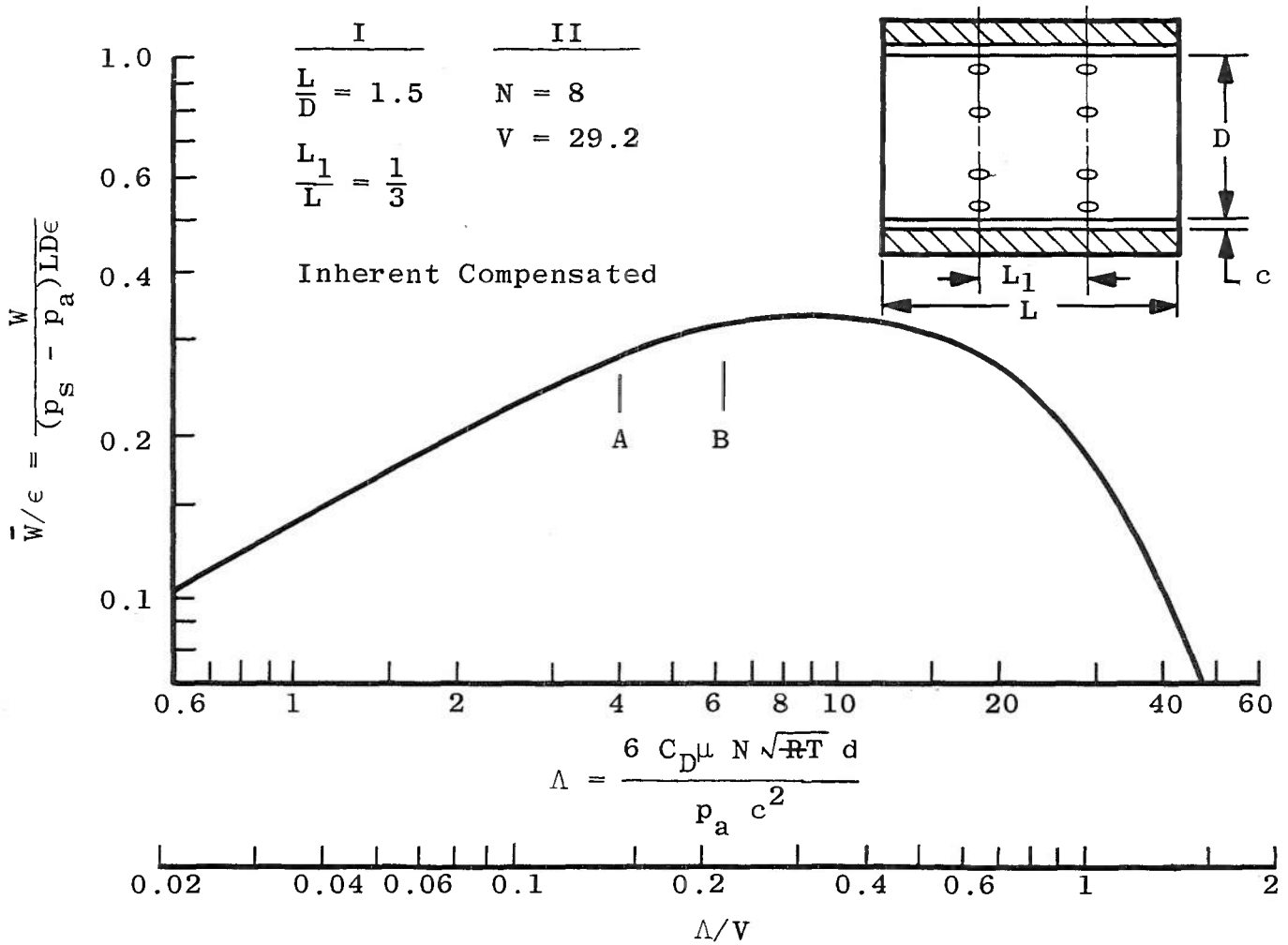

Figure 8. Typical Stiffness Curve for a Journal Bearing.

drop through the orifices (large Λ), the pressure at the inlet to the gas film is nearly the supply pressure and the pressure cannot increase significantly when the bearing is deflected. When there is a large pressure drop through the orifices (small Λ), the pressure level at the gas film inlet is so small that very little load capacity can be obtained.

For the present design, it is desirable to minimize the mass flow rate for two reasons:

1. Excessive mass flow could interfere with the model motion and thus introduce unpredictable errors in the data obtained from the balance.
2. In order to keep the Reynolds number small, the mass flow must be minimized, Equation (59).

An examination of Figure 8 reveals that to obtain near optimum stiffness and minimize mass flow rate (i.e., minimize Nd), the film thickness, c, must be minimized. The clearance is limited by manufacturing tolerances and for the present case, by the surface deflection (Figure 6, page 38). With these limitations, c was selected to be 0.001 inch.

Determination of Mass Flow and Supply Pressure

Figure 9 shows the effect of supply pressure, p_s, on the load capacity at constant mass flow rates for both single plane ($L_1 = 0$) and double plane ($L_1/L = 1/3$) admission. The ordinate in this figure is load at an eccentricity of 0.5 since Vohr [16] states that a journal bearing

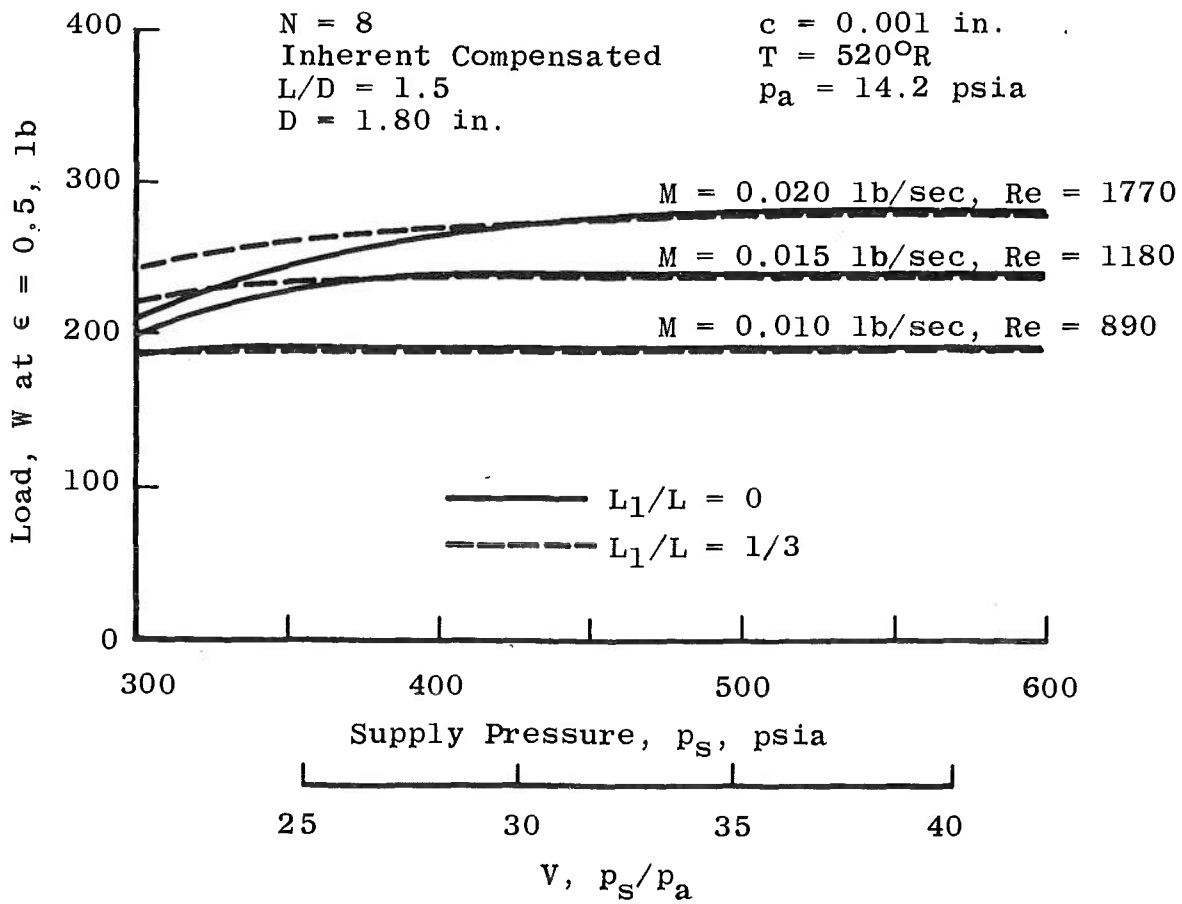

Figure 9. Effect of Supply Pressure on Load Capacity with Constant Mass Flow Rate.

cannot be expected to operate at eccentricities larger than 0.5 due to a phenomena termed "lock-up." It can be seen in Figure 9 that the load increases with supply pressure up to a given p_s, above which the load remains constant. There is little effect of single or double plane admission on maximum load capacity for the two cases shown. A more detailed discussion of admission plane location will be given later.

It is evident from Figure 9 that in order to get the load capacity required, the mass flow and thus Reynolds number must be large. If the bearings angular stiffness is neglected, each journal bearing would have to support somewhat over 350 pounds since their centers are inside the ± 0.2 inch specification. It was the opinion of the writer, based on angular stiffness data from Reference [16] and experience with a similar configuration, that a necessary and sufficient mass flow would be 0.020 lb/sec. A supply pressure of 414 psia was selected since the load has practically reached its maximum value, and larger supply pressures would increase the possibility of supersonic flow (reduced load) in the film.

Figure 10 shows the effect of the orifice plane locations on the load capacity for the selected configuration. It can readily be seen that for constant mass flow, the load capacity is practically unaffected if (L_1/L) is less than 0.4 but decreases rapidly as the orifices are moved

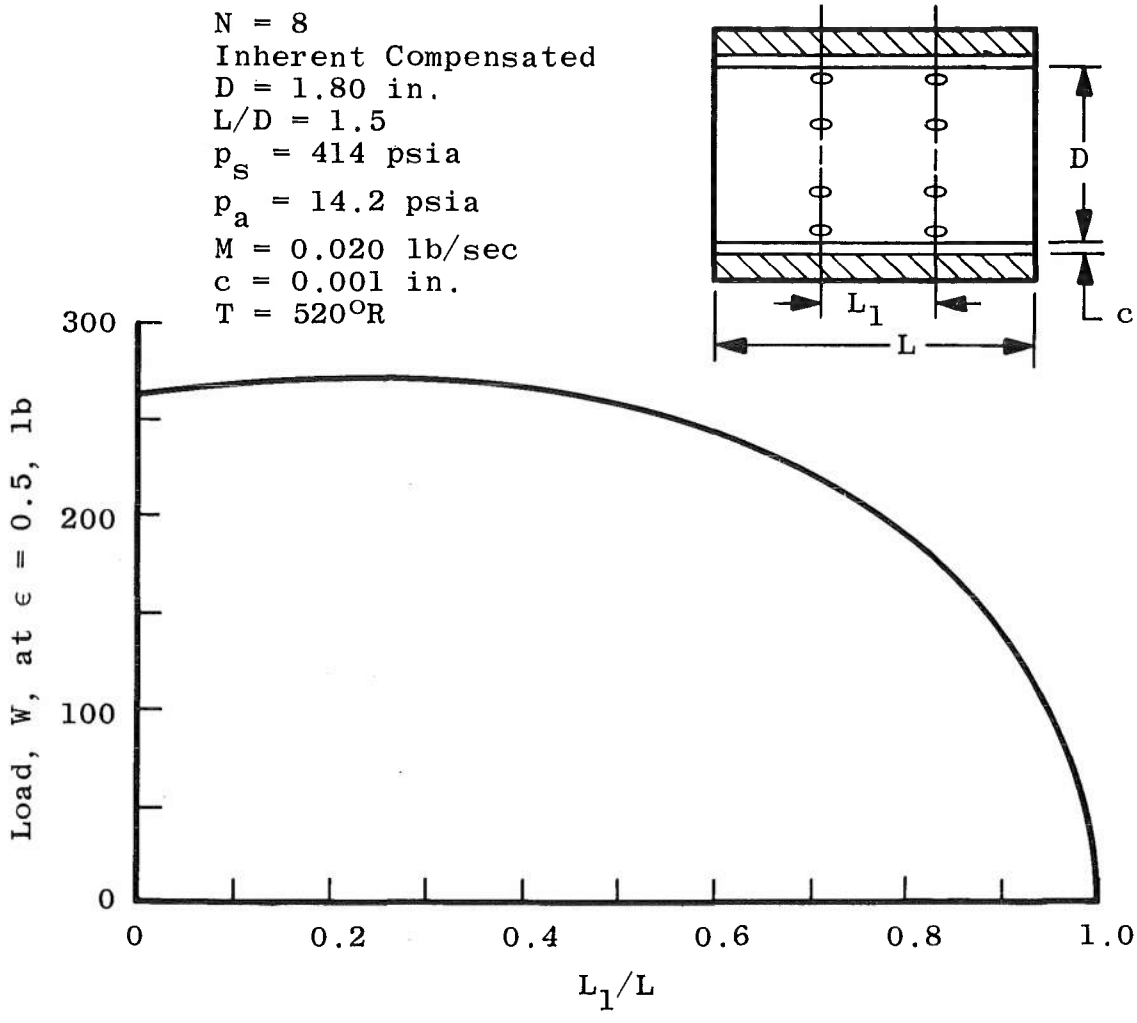

Figure 10. Effect of Separating Feeding Planes with Constant Mass Flow Rate.

further toward the ends. A value of one-third was selected for L_1/L since experience with a similar bearing had shown a slight increase in angular stiffness for a double plane admission bearing. Reference [16] shows practically the same angular stiffness for the two configurations.

Now with all the parameters selected, a major problem area could be the large film Reynolds number (Re = 1770). The present design point is designated "A" in Figure 8, page 43. From this figure the writer's first impression was that a turbulent film, if it occurred, would essentially increase Λ because of an increase in μ and a more optimum load capacity would be obtained. The modified Reynolds number, Re^*, from Equation (57) was found to be 1.75 and thus the error due to neglecting inertia effects would be small.

Orifice Type

Lund [7] has shown, theoretically, that pneumatic instability can be expected with orifice compensation at certain values of Λ and V and has presented this information as stability maps. In general the maps show that bearings which are designed for near optimum stiffness are subject to experience pneumatic hammer for values of V greater than about 10. Thus inherent compensation was used in the present design, and all of the preceding data have been for this type of orifice.

II. THRUST BEARING

Restrictor Coefficient

Figure 11 shows the stiffness versus restrictor coefficient, Λ, curve which has a characteristic optimum value similar to the journal bearing. Since the thrust bearing, unlike the journal bearing, can be analyzed for any value of eccentricity, the stiffness at $\varepsilon = 0$ was selected for use in Figure 11.

It should be noted that the curve shown is for eight orifices per side ($N = 8$) of the bearing. A discussion of the effect of N on load capacity will be given later.

The variation of the load capacity with eccentricity for three different values of Λ is shown in Figure 12. In all cases shown, the stiffness (i.e., slope of the curves) increases with ε. The stiffness (i.e., slope of the curves) is nearly constant in all cases up to $\varepsilon = 0.3$, and the variation with eccentricity becomes less as Λ gets nearer the optimum value.

As was the case for the journal bearing, it is necessary to minimize the clearance, c, to keep the mass flow down and obtain a large stiffness. Thus a value of 0.0008 inches which is feasible to fabricate was selected for c.

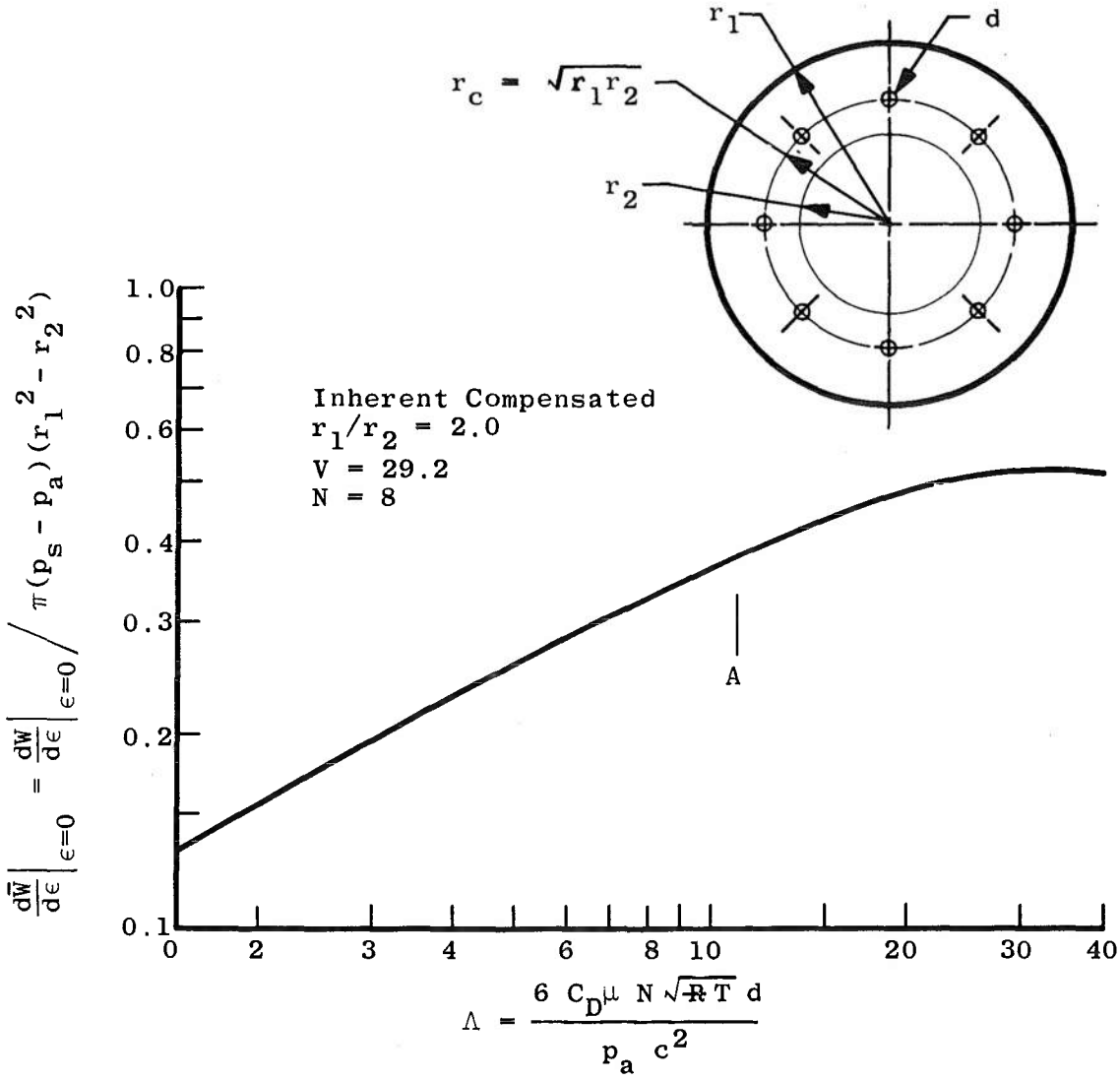

Figure 11. Effect of Restrictor Coefficient on Thrust Bearing Stiffness.

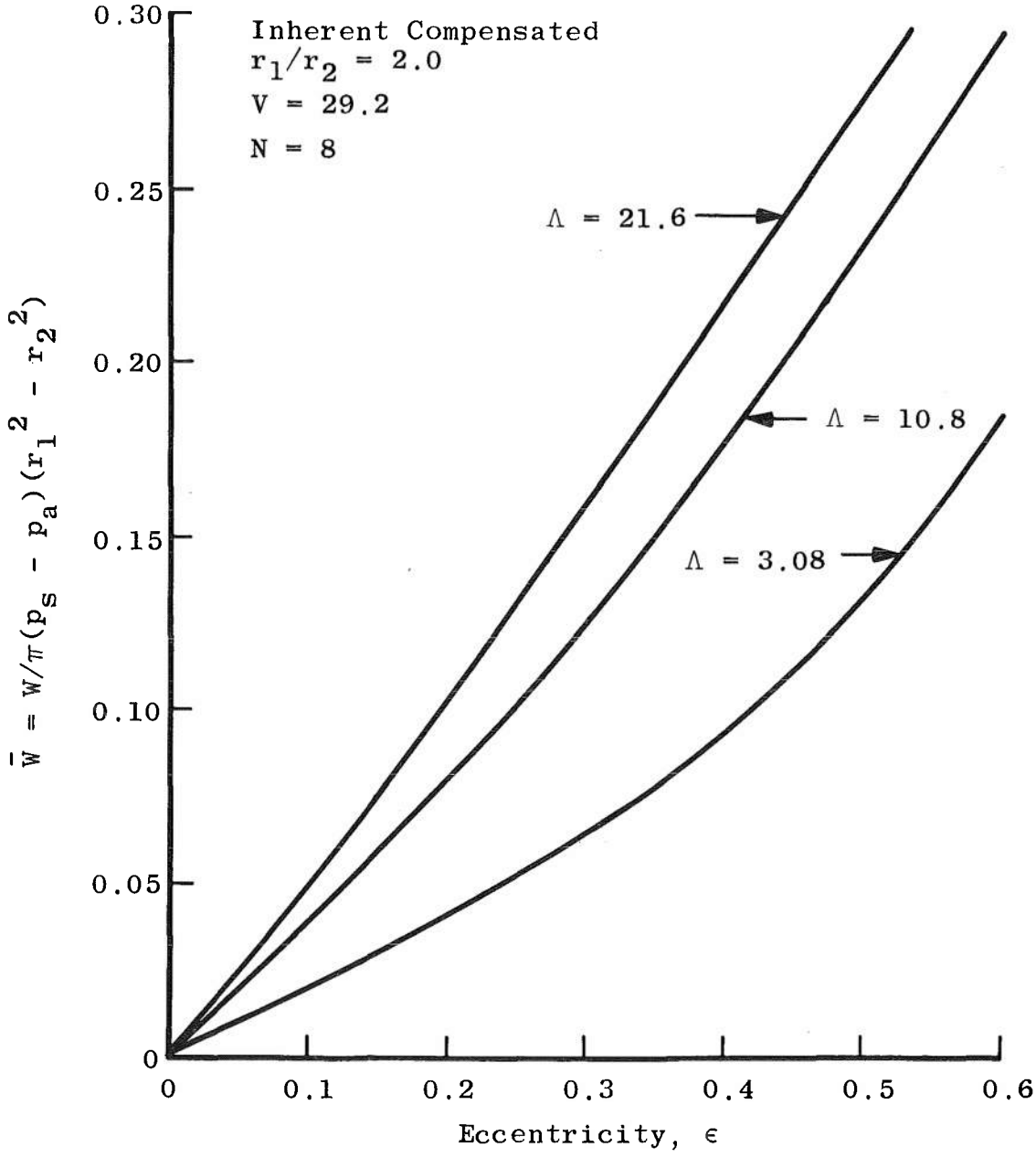

Figure 12. Variation of Load with Eccentricity.

Mass Flow

With the clearance determined, the load can be determined as a function of mass flow rate as shown in Figure 13. The load is given for a value of eccentricity of 0.5. Abscissas of Reynolds number and orifice diameters are also shown. The Reynolds number can be expressed as a function of mass flow rate, similar to Equation (59), to give

$$Re = M/8\pi\, r_c\, \mu \tag{60}$$

Point A was selected as the design point which was considerably over the 150 pound load requirement. The writer had not had any experience with this type of bearing and it was felt that a factor of safety was required for two reasons. First, there was likely to be noticeable drop in supply pressure to the thrust bearing since the flow had to pass through some small channels to arrive at the inlet orifice. Second, Vohr [22] showed that "entrance effects" can cause considerable loss in load capacity for double acting bearings. These entrance effects are more pronounced for bearings with small areas.

Number of Orifices

As previously mentioned, the number of orifices per bearing side, N, was eight. The reason for this number was that it was the maximum that could be machined without complicating the design. Figure 14 shows that the load capacity

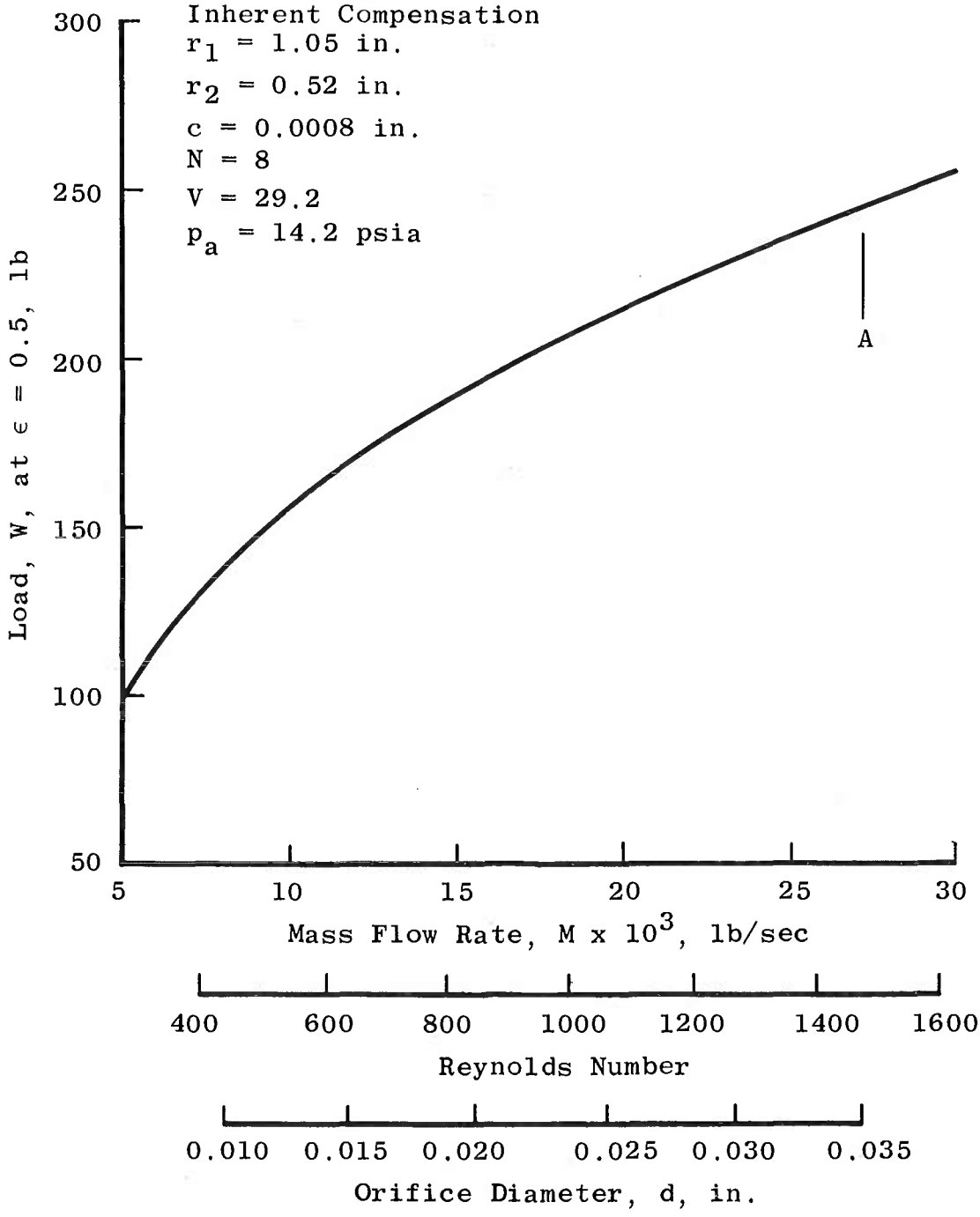

Figure 13. Effect of Mass Flow Rate on Thrust Bearing Load Capacity.

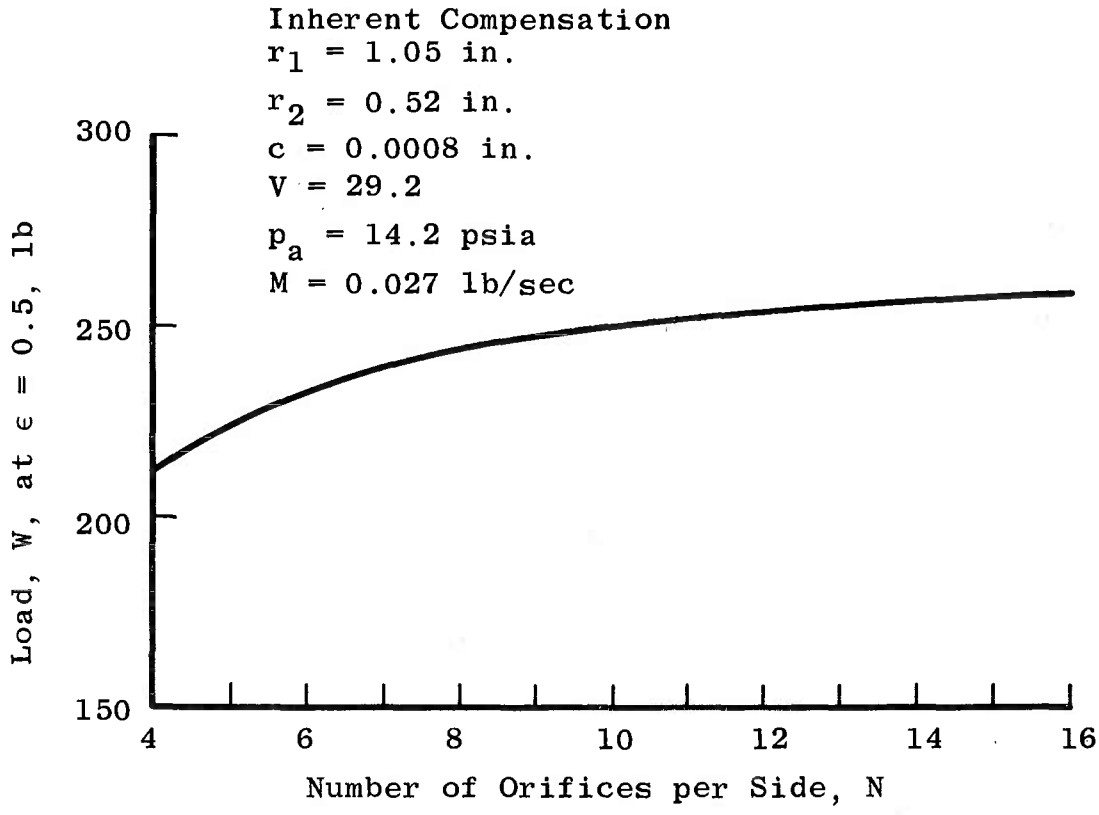

Figure 14. Effect of Number of Orifices on Thrust Bearing Load Capacity with Constant Mass Flow Rate.

for the present design increases as N is increased when the mass flow rate is fixed. There is, however, only a 5.5 percent increase in the load as N is increased from 8 to 16; and thus increasing the number of orifices above eight could not be justified.

III. BEARING DYNAMICS

A typical model that would be tested using the roll damping balance would have a mass, m, of about 0.1 lb-sec^2/in and a moment of inertia, I, about its transverse axis of about 6 in-lb-sec^2. Using these numbers along with the theoretical stiffnesses at $\varepsilon = 0$ and Equation (50), the first natural frequencies in the translational modes can be calculated to be

$$\omega_r = 3290 \text{ rad/sec} = 31{,}400 \text{ rev/min}$$

$$\omega_A = 2470 \text{ rad/sec} = 23{,}600 \text{ rev/min} .$$

If the angular stiffness of the individual bearings is neglected, the first natural frequency in the angular mode can be calculated to be

$$\omega_a = 700 \text{ rad/sec} = 6700 \text{ rev/min} .$$

If the angular stiffness obtained from [16], (454,000 in-lb/rad for each journal and 398,000 in-lb/rad for the

thrust bearing) is added to the angular stiffness due to the separated journal bearings, the angular natural frequency is increased to

$$\omega_a = 772 \text{ rad/sec} = 7720 \text{ rev/min}$$

In any case the bearing is well above the 5000 rev/min requirement.

CHAPTER IV

APPARATUS

I. GAS BEARING

The gas bearing assembly is composed of five basic components as shown in Figure 15. Figure 15a shows a photograph of the components while Figure 15b shows the bearing assembly. As aforementioned, the journal bearing core material was Kennertium-W2^{R} which has a high modulus of elasticity. The outer race, thrust bearing core, and insert were fabricated from Ferro-Tic^{R}, grade C, which is a corrosive resistant metal with excellent dimensional stability but was found to be difficult to machine. The bolt was made of stainless steel.

The design tolerances were not held very good during fabrication. Accurate measurement of the finished bearing indicated that both the gap (film thickness) and orifice diameters were considerably larger than the design values for both the journal and thrust bearings as shown in Figure 15b. There was also a considerable variation of the clearances, c, over the bearing surfaces and the measured values given are average. The finish of the bearing surfaces was supposed to be within 4 micro inches but actually was about 10 on the journal bearing surfaces. The orifices in the thrust bearing were bellmouthed with

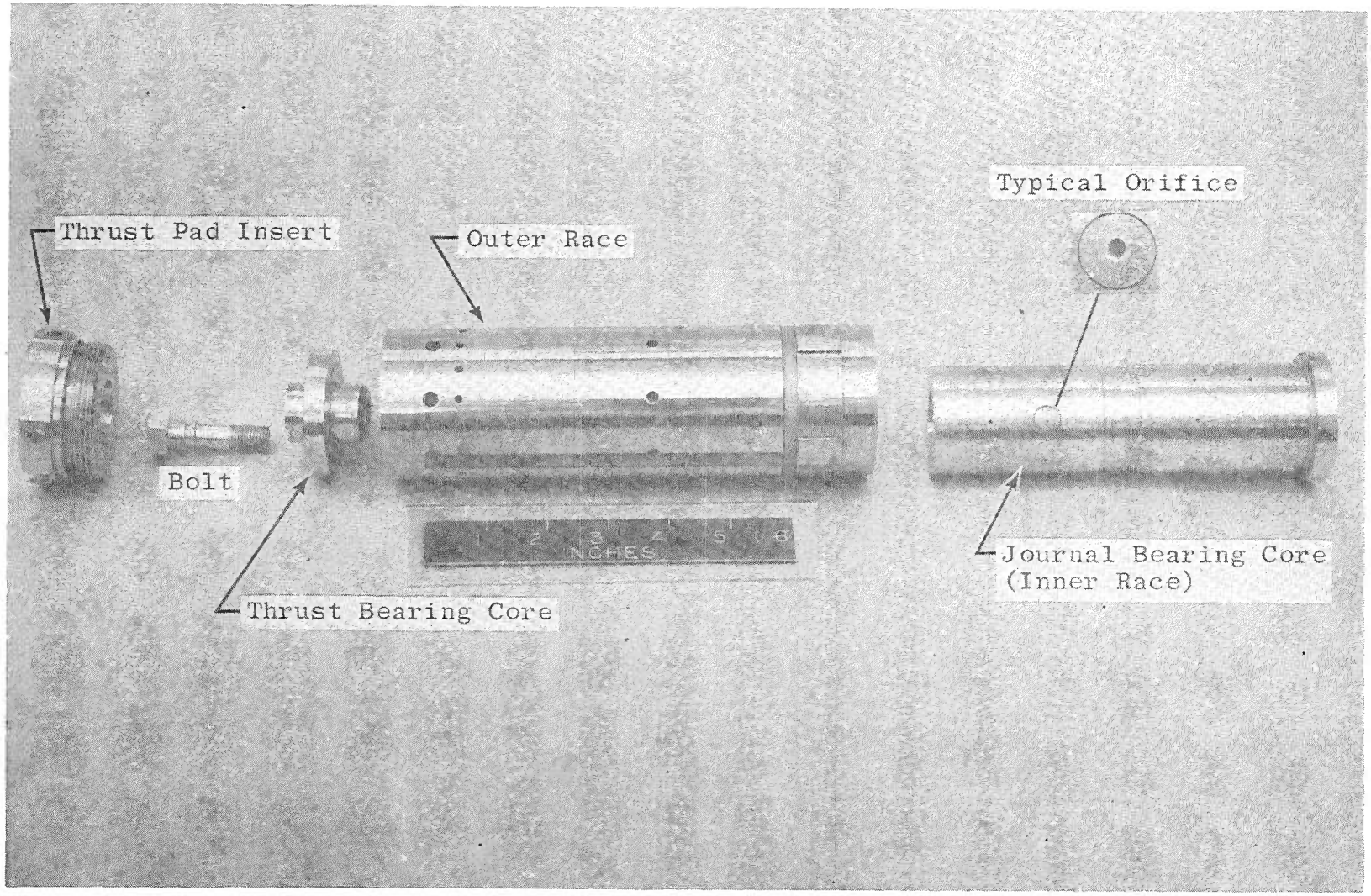

a. Photograph of components.

Figure 15. Gas Bearing Balance.

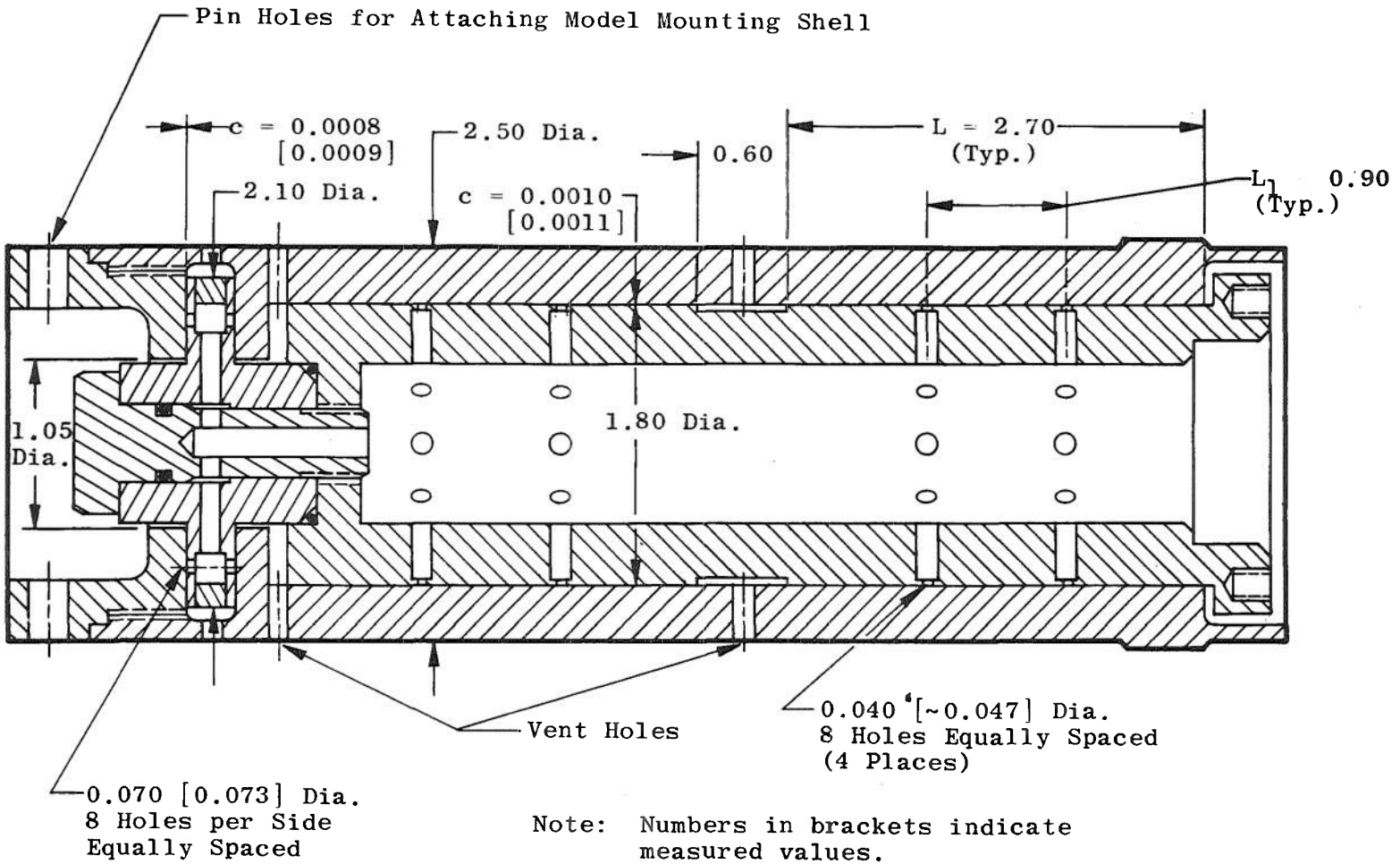

b. Gas bearing assembly.

Figure 15. (continued)

the larger diameter at the outer edge which forms the restricting area. The material, Kennertium-W2^{R}, used for the bearing core is a sintered metal and the metal flaked off at the edge of the orifice as shown on the inset in Figure 15a. An accurate measurement of the orifice diameters was impossible to obtain and the value indicated in Figure 15b was determined from mass flow measurements which will be discussed later.

II. LOADING EQUIPMENT

A photograph of the bearing with both axial and radial loads being applied is shown in Figure 16. The gas bearing was held in a support fixture. Because of the large radial loads required, a lever arrangement with a mechanical advantage of six was used to make the loading procedure easier. A mass flow meter incorporating VKF calibrated orifices, which is accurate to one percent, was installed upstream of the gas bearing. A pyrometer was used in conjunction with an iron-constanton thermocouple to monitor the temperature of the outer race.

A Sheffield^{R} air gage was used to measure the displacement of the sleeve with respect to the core within an accuracy of 0.00002 inches based on data repeatability. In order to get a good measurement of the journal bearing displacement, a pin was passed through one of the center vent holes (see inset on Figure 16) and attached to the core.

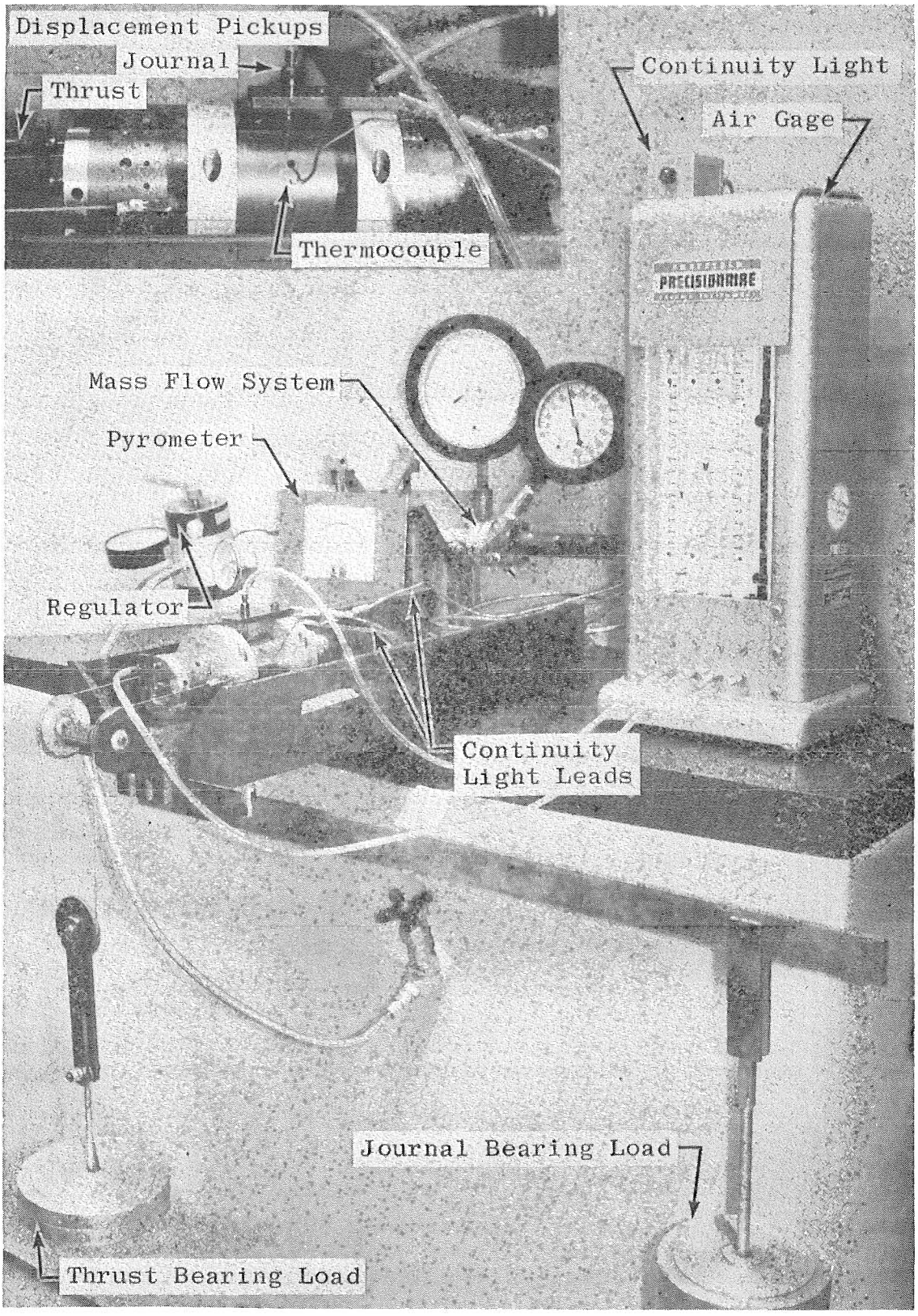

Figure 16. Photograph of Loading Apparatus.

The stylus of the air gage pickup rode on the pin while the body of the pickup was attached to the outer race. Although not shown, the thrust bearing was removed and a fixture was added so that the journal bearing core was supported from both ends when the journal displacement measurements were made. This was done in order to eliminate bending and thus obtain more reliable data that could be compared to theory. Displacement measurements were made only for a center load applied to the journal bearing. An electrical circuit was used to determine when the bearing surfaces touched. The continuity light shown in Figure 16 would indicate surface contact.

The journal bearing could be loaded at any axial location and the light observed to indicate the maximum load capacity. These measurements were made with the entire bearing assembled and cantilevered to simulate the loads that the balance would experience during a wind tunnel test program (i.e., the effects of bending included).

III. FILM PRESSURE MEASURING EQUIPMENT

A photograph of the equipment and setup used to measure the gas film pressures is shown in Figure 17. The same support structure, mass flow meter, and temperature measuring system that was discussed in the preceding section was used. A sleeve equipped with pressure ports was fabricated to fit over one of the journal bearings.

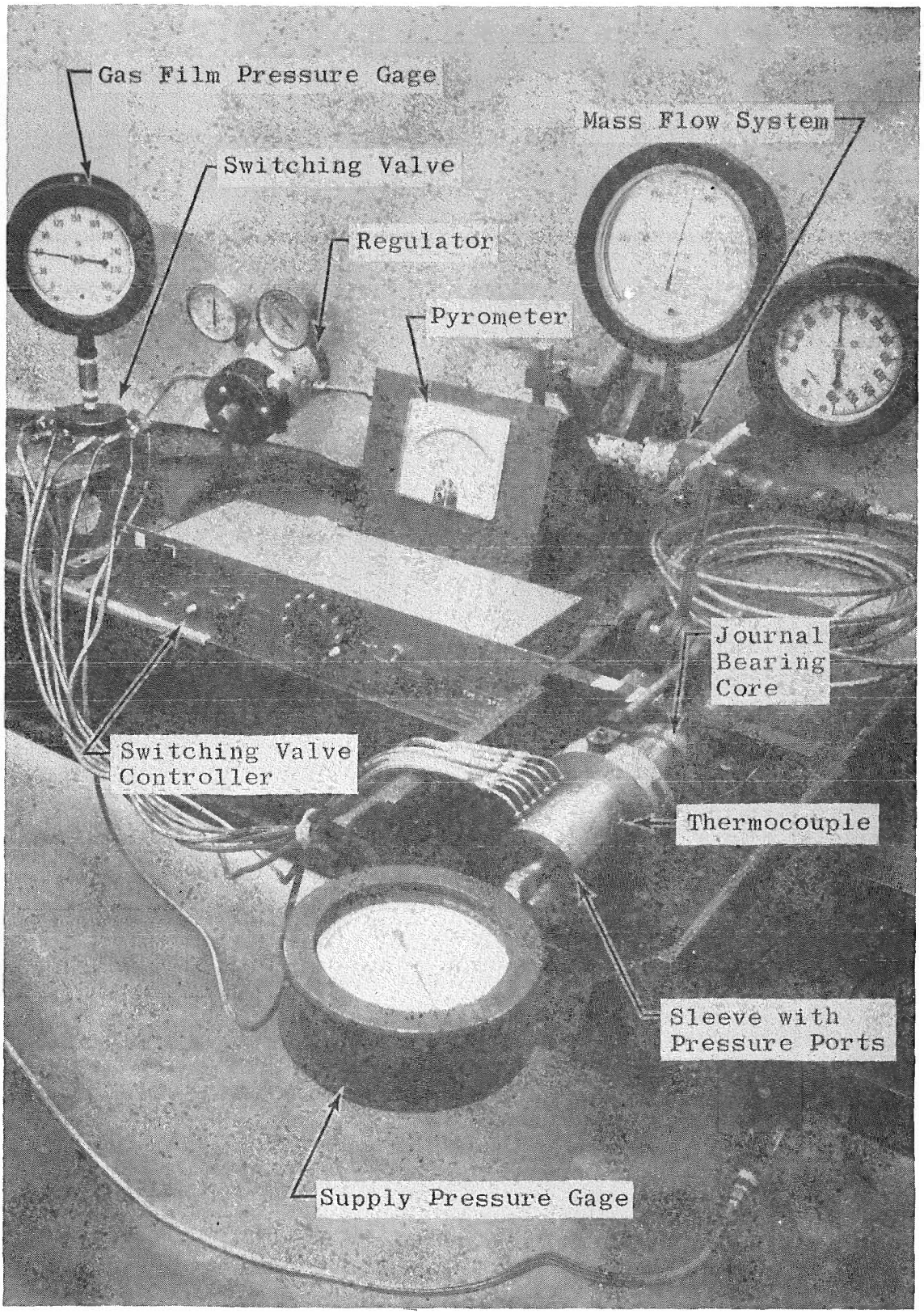

Figure 17. Photograph of Gas Film Pressure Measuring System.

The pressure ports were spaced every 0.375 inches along the length. The radial clearance between the sleeve and the core was 0.0009 inches. The orifices in the other journal were plugged during these measurements. A pressure gage was installed in the place of the thrust bearing in order to get an accurate measurement of the supply pressure. A switching valve was used to simplify the data gathering. The accuracy of the gages used to obtain the pressure measurements is estimated to within ± 2 psi.

CHAPTER V

RESULTS AND DISCUSSION

I. LOAD CAPACITY

Mass flow rate measurements at a supply pressure of 414 psia indicated the thrust bearing mass flow rate to be 0.032 lb/sec which is the value predicted from laminar theory based on actual bearing dimensions. It is important to note that the theoretical pressure ratio across the orifices is 0.35 which means the orifices are choked and the mass flow is unaffected by the downstream pressure. Thus, the agreement between theory and experiment may be misleading. The measured mass flow rate is however considerably above the design value of 0.027 lb/sec because of the machining errors. The mass flow rate per journal bearing was measured to be 0.025 lb/sec which is also much larger than the design value of 0.020 lb/sec. A theoretical value for the actual bearing could not be determined since the diameters of the orifices could not be accurately determined as mentioned in Chapter IV, Section I.

Figures 18 and 19 show the results of the load and displacement measurements of the thrust and journal bearings respectively. The journal bearing load was applied midway between the two bearings with both ends of the core supported. The load plotted in Figure 19 is one-half

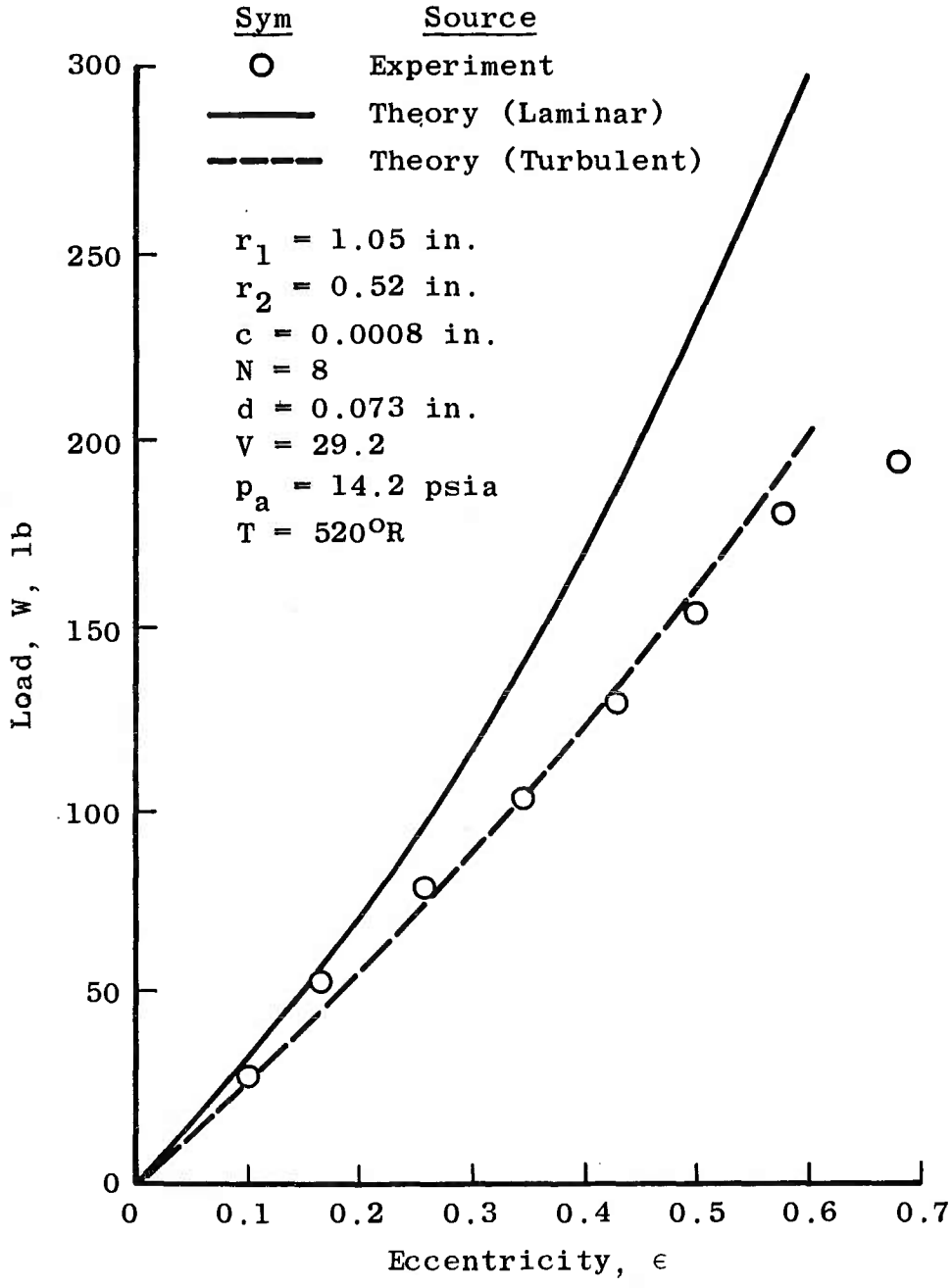

Figure 18. Thrust Bearing Load as a Function of Eccentricity.

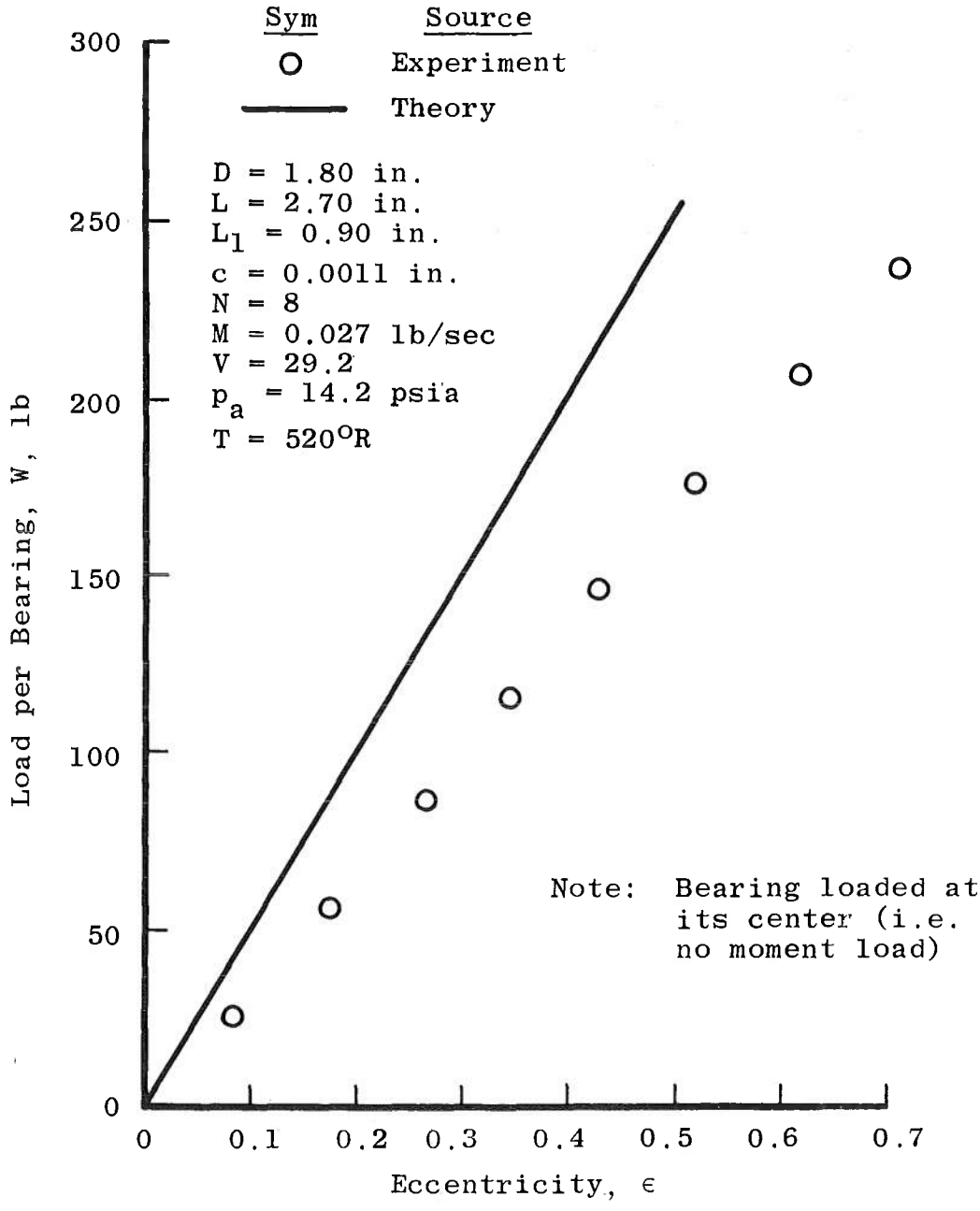

Figure 19. Journal Bearing Load as a Function of Eccentricity.

the applied load (i.e., load per bearing). It can be seen from these figures that the actual load for a given eccentricity is about 30 percent less than the value predicted from laminar flow theory. The theory shown is for the actual measured dimensions of the bearings rather than the design values. The thrust bearing theoretical stiffness was reduced about four percent from the design value while the journal bearing theoretical stiffness was practically unaffected since the restrictor coefficient was changed very little (i.e., d/c^2 was essentially unchanged from the design value). It should be noted that the thrust bearing will support its required load of 150 pounds at an eccentricity 0.5. Figure 18 also shows a curve for turbulent theory which will be discussed later.

Figure 20 shows the results of loading the journal bearings at several axial stations. The actual load is considerably below the required value when applied 2.0 inches from the bearing center. Based on the results shown in Figure 19, the bearings are operating at an eccentricity up to 0.7 before contact is made.

II. PRESSURE DISTRIBUTION

Based on the preceding results it was felt that the bearing was not performing adequately and an investigation was undertaken to determine the cause of the reduced load capacity. Journal bearing gas film pressure measurements

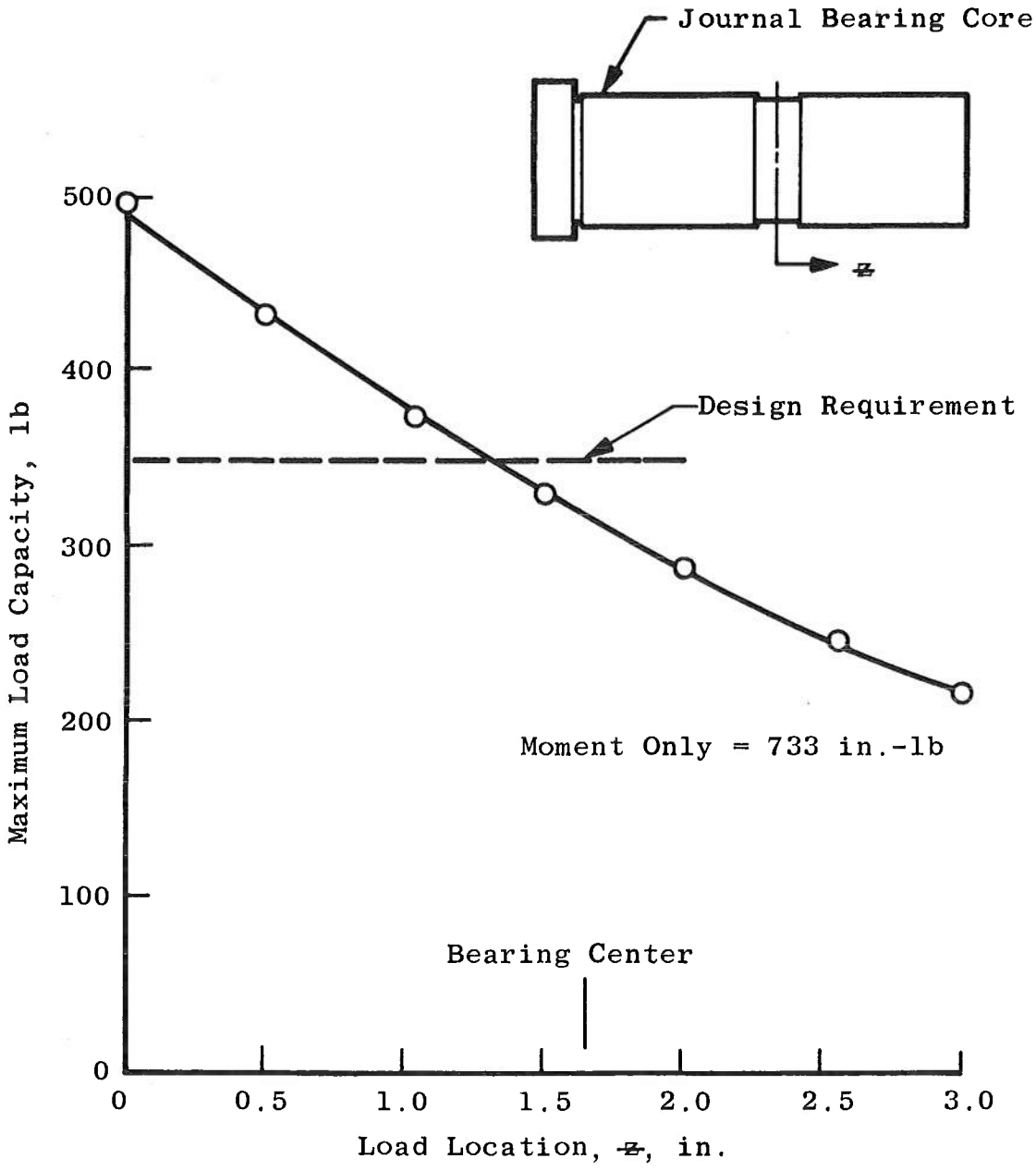

Figure 20. Maximum Journal Bearing Load Capacity as a Function of Load Location.

were made using the sleeve described in Chapter IV, Section III. First the pressure just downstream of the orifices was measured and since the mass flow rate was known, the orifice flow equation, Equation (7), could be used to determine the effective orifice size. The orifice diameter was calculated to be 0.047 inches as was previously given.

The axial pressure distribution for $\varepsilon = 0$ and $\theta = 0$ (i.e., midway between orifices) is shown in Figure 21 and reveals the pressures to be considerably greater than the level predicted by laminar flow theory. It was reasoned that in order to produce this increase in pressure, the gas film flow must be turbulent. Figure 21 shows that the pressure distribution was predicted by the laminar theory very accurately if the viscosity and thus Λ was multiplied by a factor of 1.56. However, this increase in Λ produces an increase in bearing stiffness as predicted from laminar theory which can be seen from Figure 8, page 43. Point B represents a Λ value of 1.56 times the value at point A, the design point.

To verify the existence of turbulent film flow and determine when it occurred, an experiment was conducted to determine the pressure distribution over a range of mass flow rates and thus Reynolds numbers. The mass flow rate was varied by varying the orifice diameters and also varying the supply pressures. The orifices were filled with an epoxy and drilled to various sizes. Data were taken

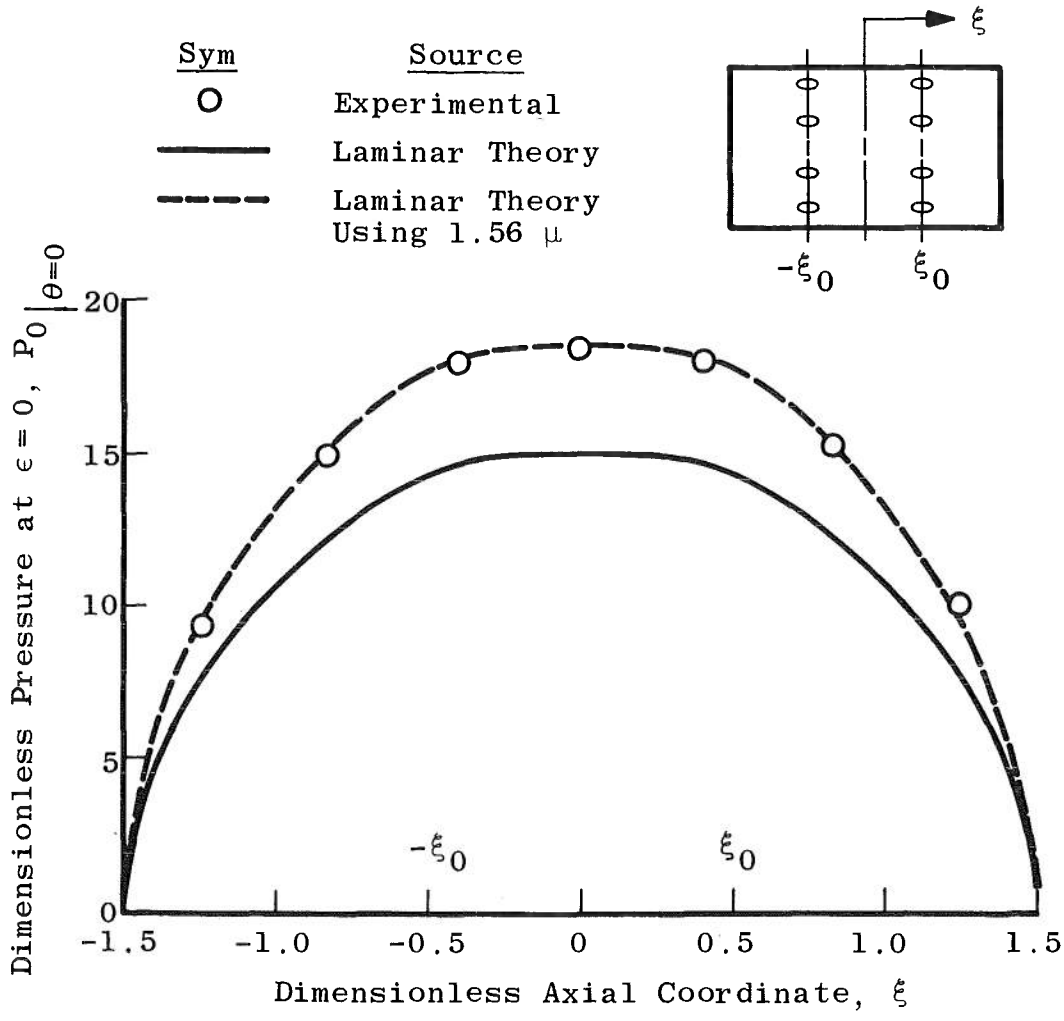

Figure 21. Journal Bearing Pressure Distribution at ε = 0.

at supply pressures of 514, 414, 314, and 214 psia. The results are shown in Figure 22. The data show good agreement with laminar theory up to a mass flow rate, m, of 1.85×10^{-6} lb-sec/in or Reynolds number of 1000. At this point the actual pressure begins to increase with m at a faster rate than that predicted by laminar theory. Shires [21] and Gross [20] showed that the gas film pressure distribution for one-dimensional, turbulent flow can be expressed as

$$(P^2 - 1)_T = \frac{0.133\ \mu^{0.25}\ RT\ (m_z')^{1.75}}{h^3\ p_a^2}\ r\left(\frac{L}{D} - \xi_>\right) \qquad (61)$$

The above equation is based on the Blasius empirical relation for shearing stress in a pipe,

$$\tau = 0.0395\ Re^{0.25}\ \rho\ V_m^2 \ . \qquad (62)$$

If Equation (61) is evaluated for the present configuration at the bearing center, the equation shown in Figure 22 for turbulent flow is obtained. It can be seen that this equation is an excellent fit of the high Reynolds number data and thus the flow must indeed be turbulent with $Re_t = 1000$. Shires [21] conducted experiments with various slot shapes at several film thicknesses and found that varying the constant in Equations (61) and (62) gave better fits with the data (a variation of approximately 12 percent was required in Shires experiments). This would be expected since the

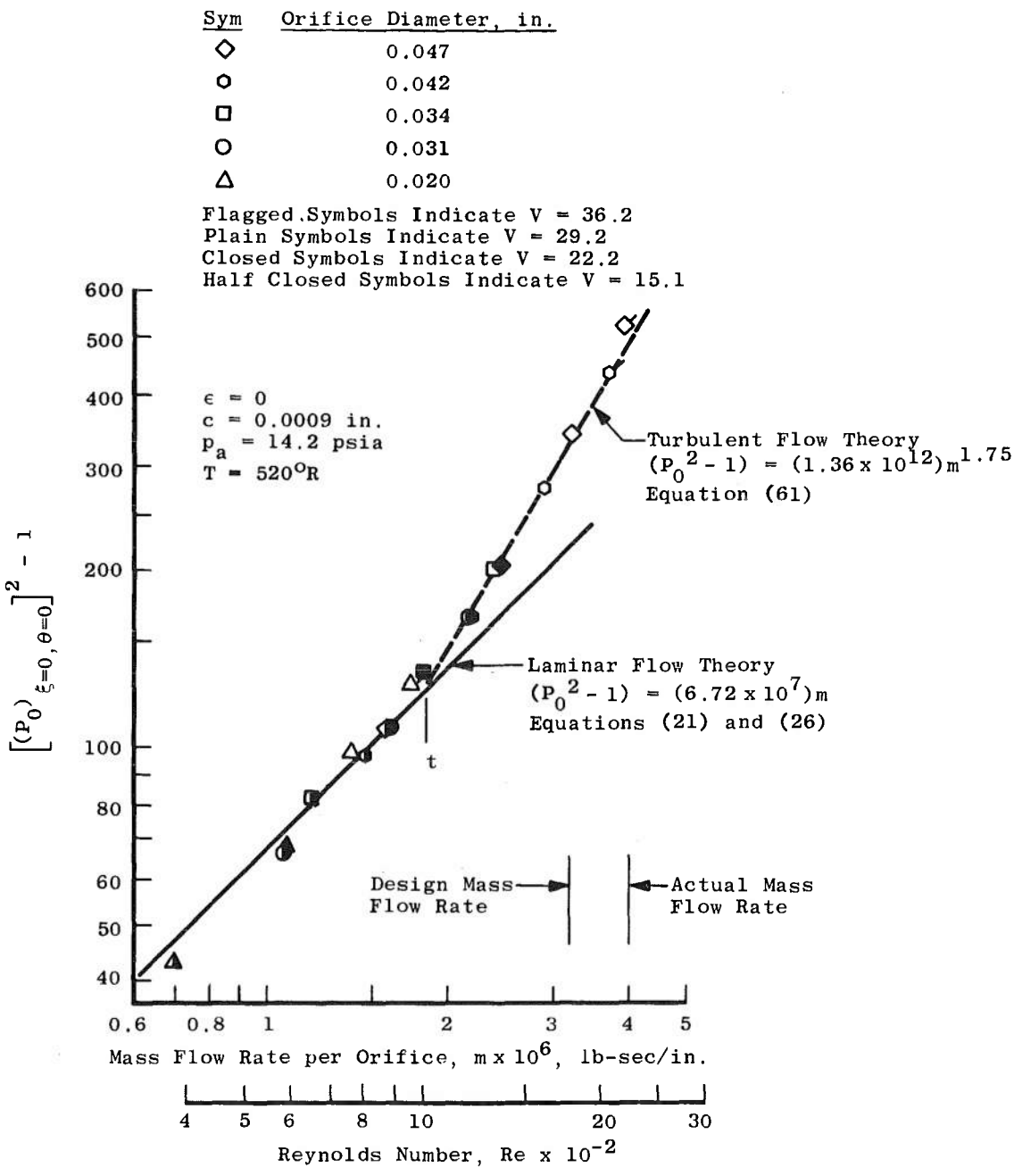

Figure 22. Effect of Film Turbulent Flow on P_0.

transition Reynolds number is subject to vary for different configurations. It is therefore somewhat fortuitous that Equation (61) provides such an exact fit of the data but the fact that $(P_0^2 - 1)$ is proportional to $m^{1.75}$ is sufficient to show that turbulent flow exists.

As given in Chapter IV, Section III, the clearance, c, obtained with the pressure sleeve installed is 0.0009 inches while the actual bearing clearance is 0.0011 inches. It is apparent from Equations (61) and (21) that the effect of changing clearance is to shift the curves along the ordinate. Shires [21] showed this to be the case if the clearance was not changed by a large amount.

III. EFFECT OF FILM TURBULENT FLOW ON LOAD CAPACITY

It would be very difficult and is beyond the scope of this study to develop a two-dimensional turbulent flow theory to determine the effects of turbulence on load capacity. However, a one-dimensional turbulent flow theory can be developed for the journal bearing to compare with 1D laminar theory. Also, the thrust bearing laminar theory can be modified slightly to give good approximate results for turbulent flow.

Journal Bearing 1D Turbulent Flow Analysis

Equation (61) can be used to develop a 1D turbulent flow theory for a journal bearing similar to the 1D laminar

theory described in Chapter II, Section I. It can be easily shown that Equation (61) can be expressed as a function of P_f instead of m_z' to produce the same result obtained in laminar theory, Equation (5). Thus the load per unit length, W', and (dW'/dP_f) for turbulent flow can be expressed the same as the laminar flow case, Equations (6) and (11) respectively.

Using Equations (7) and (61) to match mass flows yields

$$(P_f)_T^2 = \frac{\Lambda_T V^{1.75}\left[G\left(\frac{P_f}{V}\right)\right]^{1.75}(L - L_1)(1 + \varepsilon \cos\theta)^{-(1.75\ \alpha - 2.25)}}{D} + 1, \tag{63}$$

where

$$\Lambda_T = \frac{0.0665\ \mu^{0.25}(RT)^{0.125}\left[NC_D(a^2)^{(\alpha-2)}(d)^{(3-\alpha)}\right]^{1.75}}{D^{0.75}\ c^{(1.75\ \alpha - 2.25)}\ p_a^{0.25}} \tag{63a}$$

It is quite apparent that Equation (63) is considerably different from its laminar counterpart, Equation (9). The derivative of P_f with respect to ε can be obtained from Equation (63) which gives

$$\frac{1}{(1.75\ \alpha - 2.25)\cos\theta}\left(\frac{dP_f}{d\varepsilon}\right)_T\Bigg|_{\varepsilon=0} \equiv D_{2,T} = \frac{P_f^2 - 1}{2P_f}\left\{1 - \frac{1.75(P_f^2 - 1)}{2\gamma\ P_f^2} \times \left[\frac{2\gamma}{\gamma-1}\right]^{0.375}\left[\left(\frac{P_f}{V}\right)^{\frac{2}{\gamma}} - \left(\frac{P_f}{V}\right)^{\frac{\gamma+1}{\gamma}}\right]^{0.375}\left[1 + \frac{\gamma-1}{2 - 2\left(\frac{V}{P_f}\right)^{\frac{\gamma-1}{\gamma}}}\right]\right\}^{-1}, \tag{64}$$

where the term in braces is 1 for choked flow. Now Equations (10), (11), and (64) can be combined to produce an expression for the stiffness of a turbulent film

$$\left(\frac{d\bar{W}}{d\varepsilon}\right)_T\Bigg|_{\varepsilon=0} = \frac{\pi(1.75\ \alpha-2.25)}{2(V-1)}\ (D_1)\ (D_{2,T})\ , \qquad (65)$$

which is similar in form to Equation (13). Equation (65) is a function of P_f but can be related to Λ_T or mass flow by means of Equations (61) and (63). For a fixed value of P_f, the stiffness for inherent compensation can be shown from Equation (65) to be five-twelfths the stiffness for orifice compensation (i.e., $\alpha = 2$ compared to $\alpha = 3$), whereas the ratio was two-thirds for laminar flow.

A comparison of the bearing stiffness of the present journal configuration as predicted by laminar and turbulent 1D theories is shown as a function of mass flow rate in Figure 23. The mass flow rate was changed by varying the orifice diameters. It can be seen from Figure 23 that the optimum stiffness occurs at a smaller mass flow rate for turbulent flow than it does for laminar flow as would be expected. However, the peak value of the stiffness for inherent compensation is about 40 percent smaller for turbulent flow than for laminar flow. It is interesting to note that an orifice compensated bearing has about the same peak value for both turbulent and laminar flow (actually the peak value for turbulent flow is about two percent

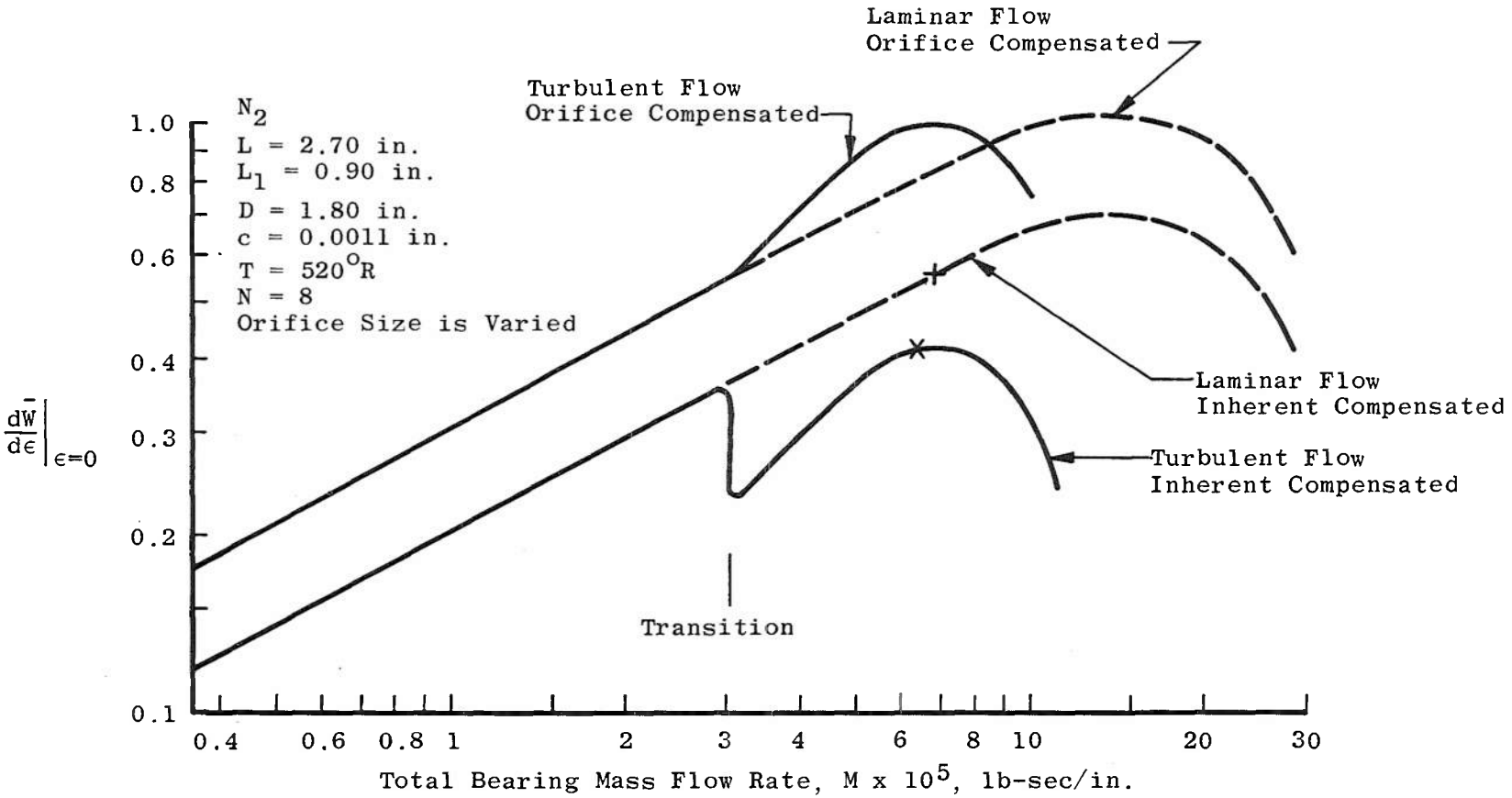

Figure 23. Effect of Film Turbulent Flow on Bearing Stiffness.

smaller). The curve for the orifice compensated bearing follows a trend that the writer originally reasoned without thoroughly investigating the effect of turbulent flow. The strong influence of the mass flow rate m_z', on the pressure for turbulent flow and the fact that the orifice area for inherent compensation varies with the clearance produced a significantly different trend of the stiffness for the present case.

The present bearing configuration is plotted on Figure 23 using an X but would be located at the point marked as + if the gas film were laminar. Although absolute levels of the stiffness is not very meaningful because 1D theory tends to overestimate stiffness, the difference in the levels should be comparable for 1D and 2D theory. The stiffness of the present bearing is shown to be about 23 percent less for turbulent flow as compared to laminar flow which is in good agreement with the 30 percent reduction found by experiment (Figure 19, page 67).

Thrust Bearing Turbulent Flow Analysis

An approximate analysis for a turbulent film in the thrust bearing can be obtained by a simple modification of the laminar theory. Since $(P^2 - 1)$ is proportional to mass flow to the 1.75 power for turbulent flow, the source strength, C, in Equation (43) can be changed to $KC^{1.75}$ for turbulent flow where K is a proportionality

constant. The proportionality constant, K, can be evaluated by equating the pressure for laminar and turbulent flow at transition, The resulting equation is

$$P_T^2 = 1 - \frac{C^{1.75}}{2C_t^{0.75}} \sum_{n=-\infty}^{\infty} (-1)^n \ln\left\{\frac{\cosh N\left[\ln R + n \ln\left(\frac{r_1}{r_2}\right)\right] - \cos N\theta}{\cosh\left[N\left(n+\frac{1}{2}\right) \ln\left(\frac{r_1}{r_2}\right)\right] - 1}\right\} \quad (66)$$

where C_t is the source strength at transition and can be determined from the transition Reynolds number for a particular bearing geometry. The source strength, C, can be determined by matching mass flows as was done for the laminar case. A fallacy in this approximate method is that the Reynolds number is not constant throughout the film and it is necessary to assume an average Reynolds number as described by Equation (60). However, it is felt for the double acting bearing that this is not a bad assumption because deviations from the average are the same on each side of the bearing and the effects tend to cancel.

This method was used to predict the load for the present bearing and is shown in Figure 18, page 66. It shows excellent agreement with the experimental data.

IV. BEARING DAMPING

The damping of the bearing with no load was determined experimentally by spinning it in a vacuum tank to a

given speed and measuring the decay in the spin rate as a function of time. It is easily shown by equating moments to angular momentum that

$$T_\omega = \frac{I \ln \left(\frac{\omega_2 - \omega_s}{\omega_1 - \omega_s}\right)}{t_2 - t_1} \tag{67}$$

The damping-moment parameter, T_ω, was found to be invarient with spin rate as theoretically predicted in Equations (54) and (56). The value of T_ω was determined to be 49.6×10^{-5} in-lb-sec/rad. The theoretical value obtained from Equations (54) and (56) using laminar viscosity is 9.1×10^{-5} in-lb-sec/rad. If 1.56 times the laminar viscosity (the effective viscosity as given in Figure 21, page 71) is used, T_ω theoretically becomes 10.9×10^{-5} in-lb-sec/rad. Since the experimental value is considerably higher than the theoretical value, the expulsion of the fairly high mass flow rate must be producing additional damping.

V. FINAL BEARING DESIGN

Design Changes

During the time this investigation was being conducted, the gas bearing was damaged in a wind tunnel test and a new bearing was to be fabricated. It was definitely desirable to have the bearing operate in the laminar flow

regime since the effect of turbulence was to decrease load capacity and increase the bearing damping. In order for the film to be laminar, the mass flow rate and thus orifice diameter, d, had to be decreased. Figure 23, page 77, shows that if only the orifice diameter of the journal bearing is decreased to the laminar flow region, there would actually be a slight loss in stiffness from the present value. However, if the clearance, c, is also decreased, the stiffness can be increased as can be seen from Figure 8, page 43. This decrease in clearance was not desirable originally because of the structural bending of the inner core, but it is felt now that the bending effect is not nearly as detrimental to load capacity as the effect of turbulence. The net effect of changing d and c was to give the final journal bearing a slightly larger theoretical stiffness as calculated from laminar flow theory.

The clearance and orifice diameters of the thrust bearing were also decreased. It was decided to decrease the orifice size a considerable amount to obtain a large reduction in mass flow. The net effect of changes in the thrust bearing design was to reduce the theoretical stiffness about 35 percent since it was felt the original conservative design was not necessary.

The only dimensions changed from the original bearing (see Figure 15b, page 59) were d and c. Since the Ferro-Tic^{R}, grade C, used for the original bearing, was very hard

to machine and also tended to rust when not maintained in a dry atmosphere, the parts made of this material were changed to stainless steel for the new bearing. The rotating parts were made from 440 B stainless while the thrust bearing core was made from Armco^{R} PH 13-8 Mo. stainless steel. The journal inner core remained Kennertium-W2^{R}. Accurate measurements of the final bearing showed that all critical dimensions were held within 25×10^{-6} inches and the bearing surface finishes were within 4 micro inches.

Calibration Results

Figure 24 shows the load versus displacement calibration for the final journal and thrust gas bearings to be in very good agreement with laminar flow theory. The mass flow rates of the journal and thrust bearings were measured to be 0.011 and 0.007 lb/sec, respectively, which are the values predicted by theory. These mass flow rates produce a Reynolds number of 970 for the journal and 390 for the thrust bearing. It can be seen from Figure 24 that the thrust bearing supports more than the 150 pound design requirement.

Figure 25 shows the results of loading the journal bearings at different axial locations. The final bearing is well within the design requirement. A fairing of the data from the initial bearing is also shown for comparison.

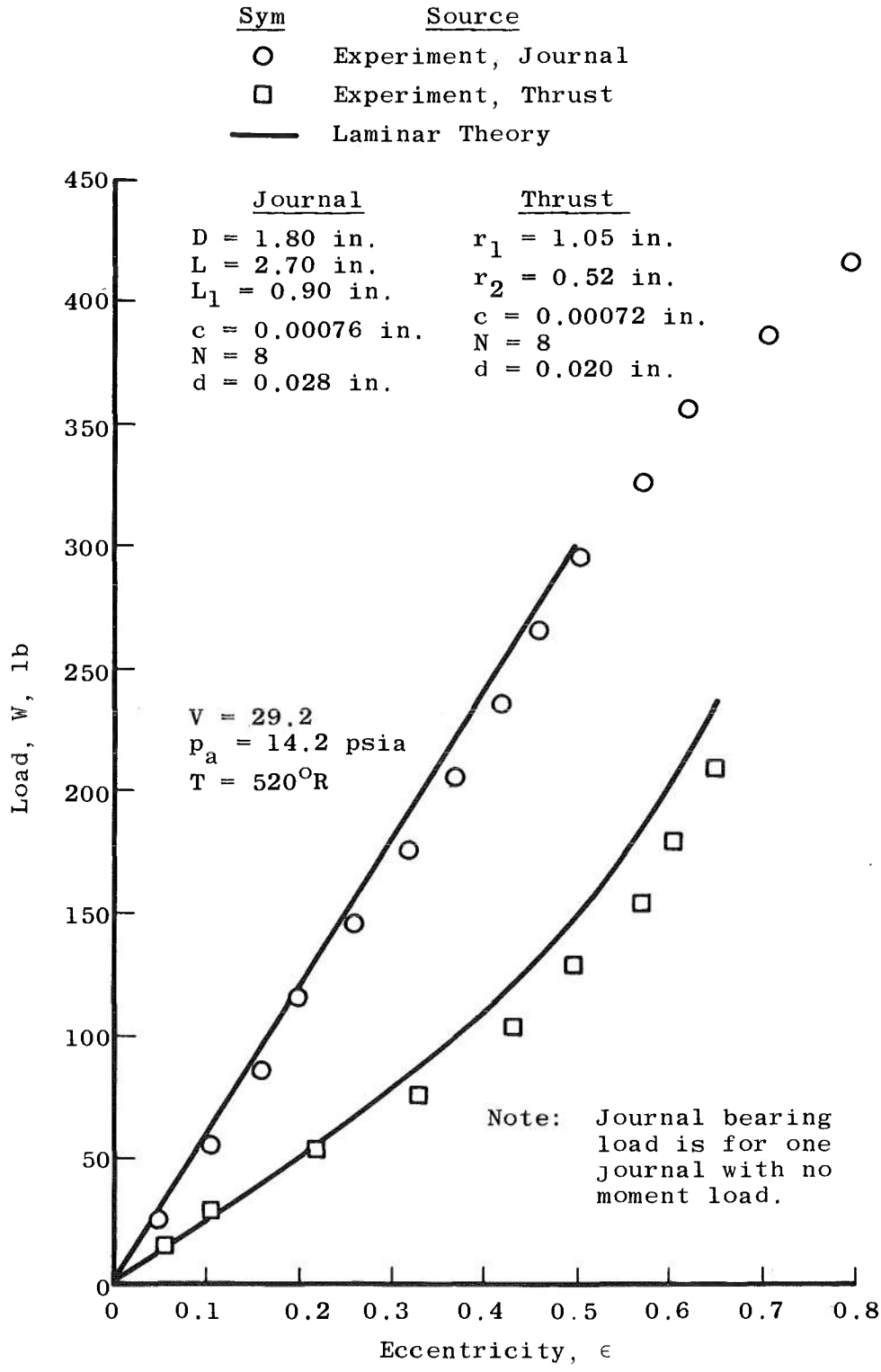

Figure 24. Variation of Journal and Thrust Bearing Loads with Eccentricity, Final Bearing.

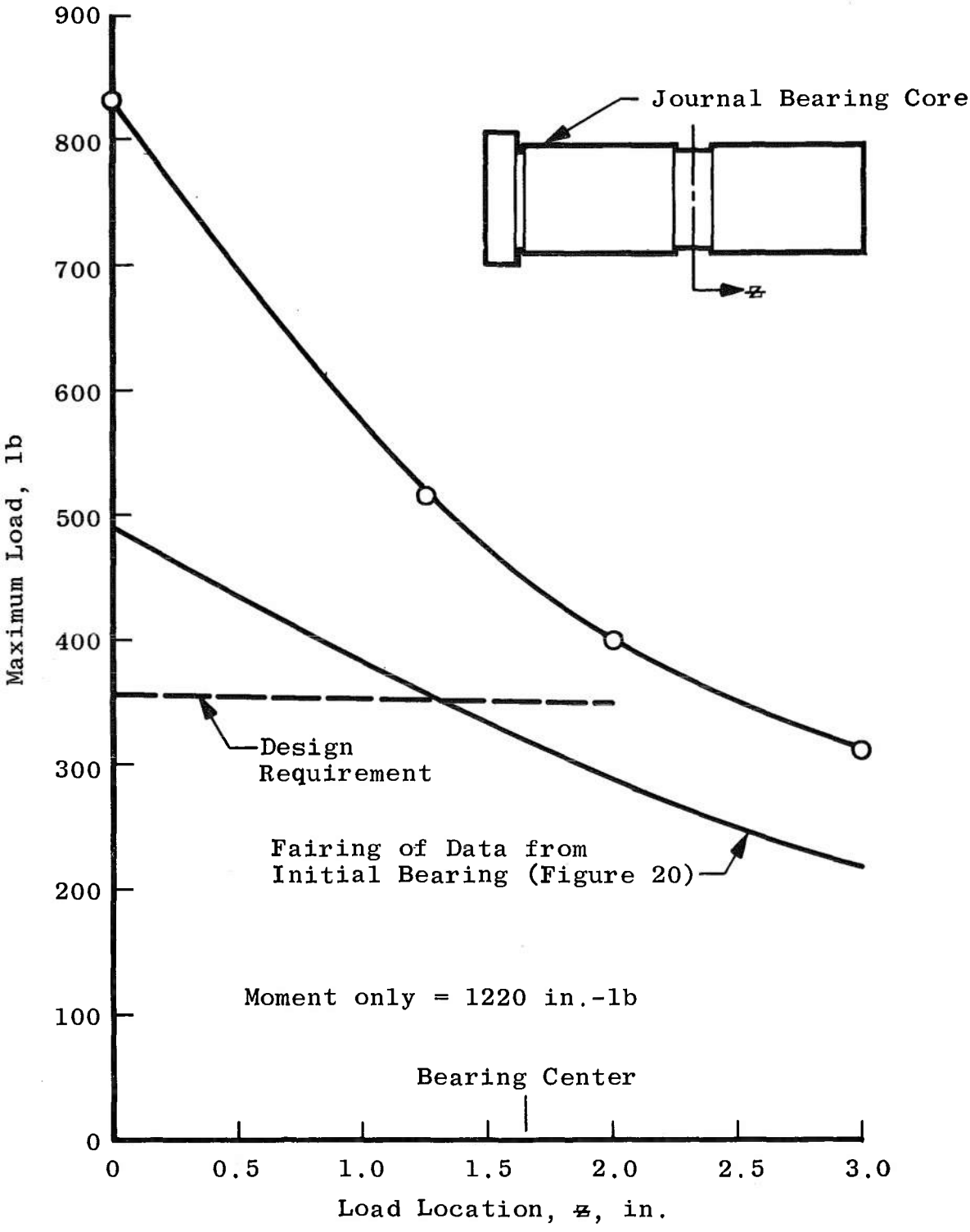

Figure 25. Variation of Journal Bearing Maximum Load Capacity with Load Location, Final Bearing.

The friction torque of the final gas bearing was measured at several mass flow rates by varying the supply pressure, p_s, to the bearing. The results are presented in Figure 26 and show T_ω to increase with mass flow rate as would be expected. The theoretical value is in good agreement with the experimental value extrapolated to zero mass flow rate. T_ω for the initial bearing is also given on Figure 26 at the operating p_s of 414 psia and is about 2.5 times greater than the value for the final bearing. A summary of the dimensions and operating characteristics of the initial and final bearings is given in Table I, page 87.

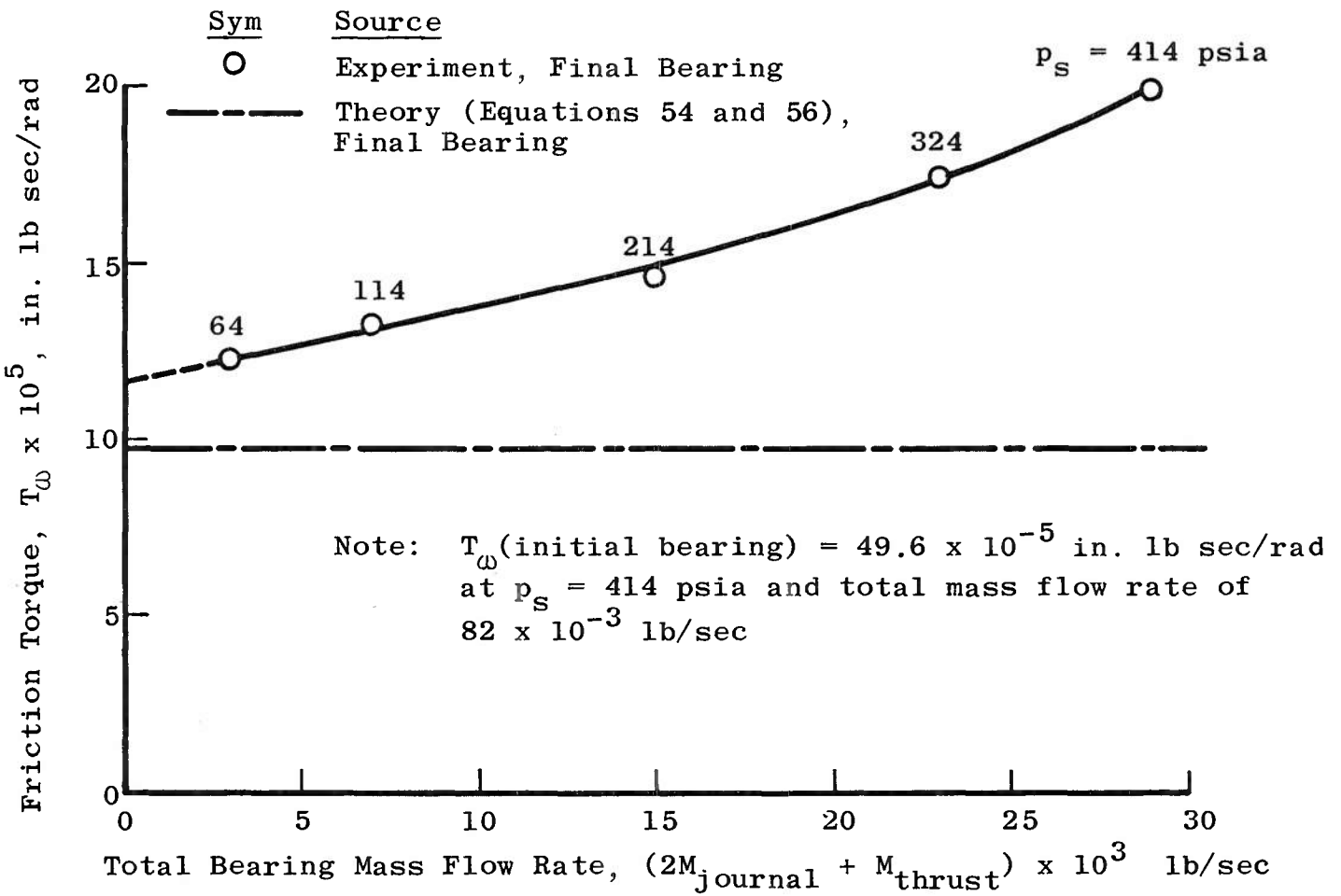

Figure 26. Effect of Mass Flow Rate on Friction Torque for the Final Bearing.

TABLE I

COMPARISON OF INITIAL AND FINAL BEARINGS

Bearing Parameter	Initial Bearing		Final Bearing	
	Journal	Thrust	Journal	Thrust
Length, L, in	2.70		2.70	
Distance between orifice planes, L_1, in	0.90		0.90	
Diameter, D, in	1.80		1.80	
Outer radius, r_1, in		1.05		1.05
Inner radius, r_2, in		0.52		0.52
Orifice diameter, d, in	0.047	0.073	0.028	0.020
Film thickness, c, in	0.0011	0.0009	0.00076	0.00072
Number of orifices, N	8	8	8	8
Temperature, T, °R	520	520	520	520
Supply pressure, p_s, psia	414	414	414	414
Ambient pressure, p_a, psia	14.2	14.2	14.2	14.2
Restrictor coefficient, Λ	3.88	9.02	4.85	3.86
Mass flow rate, M, lb/sec	0.025	0.032	0.011	0.007
Film Reynolds number, Re	2200	1780	970	390
Stiffness @ ε=0, K, lb/in	313,000	334,000	755,000	342,000
Load @ ε=0.5, $W\big\vert_{\varepsilon=0.5}$, lb	170	150	290	135
Friction torque, T_ω, in-lb-sec/rad	49.6×10^{-5}		19.9×10^{-5}	

CHAPTER VI

SUMMARY

Externally pressurized journal and thrust gas bearings were designed for use as a roll damping, wind tunnel balance. In order to be small in size and support the required loads necessitated that the bearings operate at large film Reynolds numbers. The first design resulted in a turbulent film. A theoretical and experimental investigation produced the following results:

1. The fact that the square of the film pressure is a linear function of the mass flow rate for laminar flow and is a function of mass flow rate to the 1.75 power for turbulent flow was verified.
2. Turbulent flow can be expected at film Reynolds numbers above 1000.
3. The maximum stiffness for a given gas bearing configuration occurs at a smaller mass flow rate for turbulent flow than for laminar flow.
4. The maximum stiffness value is practically the same for laminar and turbulent flow if the bearing is orifice compensated whereas the value is considerably reduced for turbulent flow if the bearing is inherent compensated.

5. It is well known that the stiffness ratio of inherent to orifice compensation for laminar flow is two-thirds. It was shown in this investigation that the theoretical ratio for turbulent flow is five-twelfths.

Since it was necessary to design the bearings with inherent compensation to avoid pneumatic hammer instability, the resulting turbulent flow of the original bearing caused it to fall below the design requirements. A new bearing was designed and fabricated to operate in the laminar flow regime. The results from this bearing showed the operating characteristics to be much better than the original bearing and was in good agreement with laminar flow theory.

BIBLIOGRAPHY

1. Schueler, C. J., L. K. Ward, and A. E. Hodapp, Jr. "Techniques for Measuring Dynamic Stability Derivatives in Ground Test Facilities." AGARDograph 121, NASA, Langley Field, Virginia, October, 1967.

2. Hodapp, A. E., Jr. "Evaluation of a Gas Bearing Pivot for a High Amplitude Dynamic Stability Balance," Arnold Engineering Development Center TDR-62-221, Arnold Air Force Station, Tennessee, December, 1962.

3. Hodapp, A. E., Jr. "A Theoretical and Experimental Investigation of a Spherical Gas Journal Bearing." Unpublished Master's thesis, The University of Tennessee, Knoxville, 1967.

4. Hersey, Mayo Dyer. Theory and Research in Lubrication. New York, London, Sydney: John Wiley and Sons Incorporated, 1966.

5. Vohr, J. H. "Restrictor Flows," Design of Gas Bearings, N. F. Reiger, editor. Vol. I. Latham, New York: Mechanical Technology Incorporated, 1966. Pp. 5.1.1-5.1.21.

6. Grinnel, S. K., and H. H. Richardson. "Design Study of a Hydrostatic Gas Bearing with Inherent Orifice Compensation," Transactions of the American Society of Mechanical Engineers, 79:11-21, January, 1957.

7. Lund, J. W. "Dynamic Performance and Stability," Design of Gas Bearings, N. F. Reiger, editor. Vol. I. Latham, New York: Mechanical Technology Incorporated, 1966. Pp. 5.8.1-5.8.30.

8. Richardson, Herbert H. "Static and Dynamic Characteristics of Compensated Gas Bearings," Transactions of the American Society of Mechanical Engineers, 80:1503-1509, October, 1958.

9. Chiang, T., and C. H. T. Pan. "Analysis of Pneumatic Hammer Instability of Inherently Compensated Hydrostatic Thrust Gas Bearings," Mechanical Technology Incorporated Report 66TR47, Latham, New York, January, 1967.

10. Tang, I. C., and W. A. Gross. "Analysis and Design of Externally Pressurized Gas Bearings," Transactions of the American Society of Lubrication Engineers, 5:261-284, April, 1962.

11. Dudgeon, E. H., and I. R. G. Lowe. "A Theoretical Analysis of Hydrostatic Gas Journal Bearings," National Research Council Report MT-54, Ottawa, Canada, August, 1965.

12. Grinnell, S. K. "Flow of a Compressible Fluid in a Thin Passage," Transactions of the American Society of Mechanical Engineers, 78:765-771, May, 1956.

13. Robinson, C. H., and F. Sterry. "The Static Strength of Pressure Fed Gas Journal Bearings, Jet Bearings," Atomic Energy Research Establishment Report R/R 2642, Harwell, Berkshire, England, September, 1958.

14. Shires, G. L. "The Design of Externally Pressurized Bearings," Gas Lubricated Bearings, N. S. Grassam and J. W. Powell, editors. London: Butterworth and Co. Ltd., 1964. Pp. 110-139.

15. Lund, J. W., R. J. Wernick, and S. B. Malanoski. "Analysis of the Hydrostatic Journal and Thrust Gas Bearing for the NASA AB-5 Gyro Gimbal Bearing," Mechanical Technology Incorporated Report 62TR26, Latham, New York, October, 1962.

16. Vohr, J. H. "Journal Bearings," Design of Gas Bearings. N. F. Reiger, editor. Vol. I. Latham, New York: Mechanical Technology Incorporated, 1966. Pp. 5.5.1-5.5.30.

17. Pan, C. H. T. "Hybrid Journal Bearings," Design of Gas Bearings, N. F. Reiger, editor. Vol. I. Latham, New York: Mechanical Technology Incorporated, 1966. Pp. 5.6.1-5.6.15.

18. Gross, W. A. "Externally Pressurized Bearing Lubrication," Proceedings International Symposium of Lubrication and Wear, D. Muster and B. Sternlicht, editors. Berkeley, California: McCutchan Publishing Corporation, 1965. Pp. 307-421.

19. Constantinescu, V. N. "Theory of Turbulent Lubrication," Proceedings International Symposium of Lubrication and Wear, D. Muster and B. Sternlicht, editors. Berkeley, California: McCutchan Publishing Corporation, 1965. Pp. 153-213.

20. Gross, W. A. Gas Film Lubrication. New York, London: John Wiley and Sons Incorporated, 1962.

21. Shires, G. L. "The Viscid Flow of Air in a Narrow Slot," Aeronautical Research Council Current Paper, No. 13, London, England, 1950.

22. Vohr, J. H. "An Experimental Study of Flow Phenomena in the Feeding Region of an Externally Pressurized Gas Bearing," Mechanical Technology Incorporated Report 65TR47, Latham, New York, July, 1966.

UNCLASSIFIED

Security Classification

DOCUMENT CONTROL DATA - R & D

(Security classification of title, body of abstract and indexing annotation must be entered when the overall report is classified)

1. ORIGINATING ACTIVITY *(Corporate author)*
Arnold Engineering Development Center
ARO, Inc., Operating Contractor
Arnold Air Force Station, Tennessee

2a. REPORT SECURITY CLASSIFICATION
UNCLASSIFIED

2b. GROUP
N/A

3. REPORT TITLE

DESIGN OF A WIND-TUNNEL ROLL-DAMPING BALANCE INCORPORATING EXTERNALLY PRESSURIZED GAS BEARINGS OPERATING AT LARGE FILM REYNOLDS NUMBERS

4. DESCRIPTIVE NOTES *(Type of report and inclusive dates)*
Final Report - August 1966 - August 1969

5. AUTHOR(S) *(First name, middle initial, last name)*

G. E. Burt, ARO, Inc.

6. REPORT DATE	7a. TOTAL NO. OF PAGES	7b. NO. OF REFS
October 1969	107	22

8a. CONTRACT OR GRANT NO.	9a. ORIGINATOR'S REPORT NUMBER(S)
F40600-69-C-0001	
b. PROJECT NO. G226	AEDC-TR-69-204
c. Program Element 65401F	9b. OTHER REPORT NO(S) *(Any other numbers that may be assigned this report)*
d. Program 876A	N/A

10. DISTRIBUTION STATEMENT
This document has been approved for public release and sale; its distribution is unlimited.

11. SUPPLEMENTARY NOTES	12. SPONSORING MILITARY ACTIVITY
Available in DDC	Arnold Engineering Development Center, Air Force Systems Command, Arnold Air Force Station, Tennessee

13. ABSTRACT

A roll damping, wind tunnel balance consisting of journal and thrust gas (N_2) lubricated bearings was designed for use in the von Kármán Gas Dynamics Facility's continuous flow tunnels at the Arnold Engineering Development Center. The balance was designed to be contained in a space envelope of 2.5 inches in diameter and 8.0 inches long. It was required to support a radial load of 350 pounds located ±2 inches from the journal bearing center and a thrust load of 150 pounds. In order to meet these specifications, the bearings had to be designed with large gas film Reynolds numbers where the assumptions of laminar flow and negligible inertia of the gas used in lubrication theory may be invalid. An experimental investigation of the bearing resulting from the initial design showed it to have a turbulent gas film which caused an unexpected detrimental effect on load capacity. A more thorough theoretical analysis was conducted to determine the effects of turbulent flow on gas bearing load capacity. Another bearing was designed and fabricated to operate in the laminar flow regime which improved the operating characteristics and was in good agreement with laminar flow theory.

DD FORM 1 NOV 65 1473

UNCLASSIFIED

Security Classification

14. KEY WORDS	LINK A		LINK B		LINK C	
	ROLE	WT	ROLE	WT	ROLE	WT
wind tunnels						
wind tunnel balances						
gas bearings						
journal bearings						
turbulent flow						
thrust bearings						
roll						
damping						
Reynolds number						